energies

MDPI

Review

Recent Developments and Trends in High-Performance PMSM for Aeronautical Applications

Chendong Liao [1,2], Nicola Bianchi [2,*] and Zhuoran Zhang [1,*]

[1] Department of Electrical Engineering, Nanjing University of Aeronautics and Astronautics, Nanjing 210016, China; chendongliao@nuaa.edu.cn
[2] Department of Industrial Engineering, University of Padova, 35131 Padova, Italy
* Correspondence: nicola.bianchi@unipd.it (N.B.); apsc-zzr@nuaa.edu.cn (Z.Z.)

Abstract: Permanent magnet synchronous machines (PMSMs) have been widely used in various applications such as robotics, electric vehicles, and aerospace due to their fast dynamic response, high-power/torque density, and high efficiency. These features make them attractive candidates for aeronautical applications, where the weight and volume of onboard systems are critically important. This paper aims to provide an overview of recent developments in PMSMs. Key design considerations for aeronautical PMSMs across different applications are highlighted based on the analysis of industrial cases and research literature. Additionally, emerging techniques that are vital in enhancing the performance of aeronautical PMSMs are discussed.

Keywords: permanent magnet synchronous machine; more electric aircraft; aeronautic; electromagnetic materials; addictive manufacturing; thermal management

1. Introduction

Electric power has been used in aircraft since the first ever powered flight made by the Wright brothers where electrical power is used to ignite the engine [1]. With the development of power electronic devices and new control techniques, more electrical subsystems dedicated to flight control and the well-being of passengers and cargo are integrated into the aircraft [2]. Furthermore, the trend of replacing hydraulically, pneumatically, and mechanically powered subsystems with electrically driven systems has become popular due to the potential for reducing overall weight, maintenance cost, carbon emissions, and increasing fuel economy. This concept termed "More Electric Aircraft" (MEA) brings more opportunities as well as challenges to electric machine systems.

A typical architecture of MEA is shown in Figure 1. As shown by the figure, electric machines perform various functions. Mostly, they serve as a motor to drive a load such as the hydraulic pump, the high-speed compressor, and even the main jet engine before it reaches self-sustainable speed. Some, as indicated in the figure are used as generators powered by turbines such as the ram air turbine, the engine, and the auxiliary power unit (APU) gas turbine. It can be concluded that electric machines are playing a very important role in more MEAs.

As a result of the new developing trend of MEA, both the onboard power demand and the capacity of the generator have been increasing rapidly from several hundred kilovolt-ampere before World War II to megavolt-ampere over the last several decades. An example of the typical power requirements of the aircraft subsystems is shown in Table 1 to give a quantitative view of the electrical power demands in modern MEA. Another example is the APU in modern MEA which can be designed to produce up to 450 kVA of electricity. In the future, considering the implementation of other more power-consuming loads such as laser weapons, the power capacity on an aircraft is predicted to exceed 10 megavolt-amperes.

Citation: Liao, C.; Bianchi, N.; Zhang, Z. Recent Developments and Trends in High-Performance PMSM for Aeronautical Applications. *Energies* **2024**, *17*, 6199. https://doi.org/10.3390/en17236199

Academic Editor: Ahmed Abu-Siada

Received: 1 November 2024
Revised: 22 November 2024
Accepted: 24 November 2024
Published: 9 December 2024

Table 1. Subsystem power exemplar requirements [3].

Subsystem	Commercial Aircraft
Flight Control	80 kW
Fuel Pumps	10 kW
Environmental Control System	400 kW
Avionics	10 kW
Payloads/Passenger	40 kW
Misc subsystem	310 kW
Total	850 kW

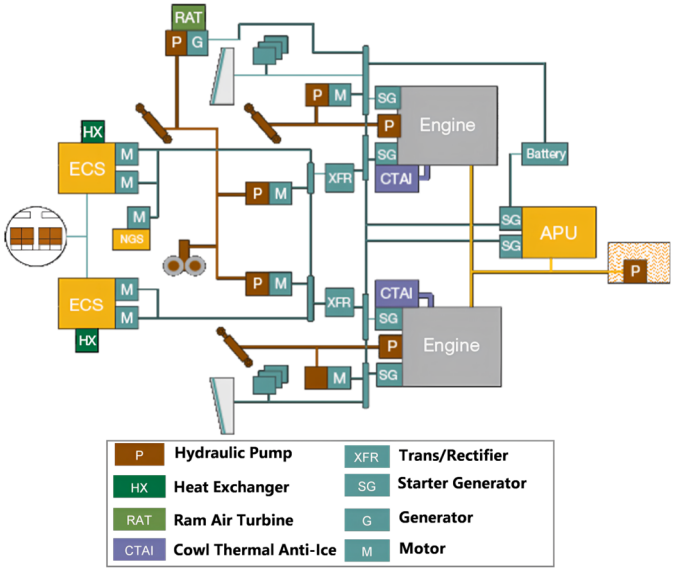

Figure 1. The No-bleed architecture of the MEA Boeing 787 Dreamliner [4].

Increased power capacity will inevitably increase the overall weight and volume of the aircraft power system due to both the increased sizes of the electric machines and drives, and the increased cross-section of the power transmission lines. This increased weight will lead to a significant increase in fuel consumption since they will be carried on the aircraft during the flight even if the machines are not working. So the top priority is to make sure that these electrical components are compact and light enough to overcome the negative effect of the additional weight and volume introduced by themselves while producing enough amount of power efficiently.

Yet by far, the propulsion power of the commercial airliners comes mainly from fuel-powered jet engines. The combustion of engine fuels not only brings greenhouse gas emissions but also changes the upper atmosphere. According to a report published by the Intergovernmental Panel on Climate Change in 1999 [5], the aviation industry presents potentially significant and increasing forcing of climate change which can be devastating to the ecosystems.

Improving the efficiency of jet engines and finally getting rid of the engine fuel is the major obstacle to achieving the ultimate goal of net zero-carbon emission. Therefore using electric motors to provide thrust force for the aircraft has drawn more and more attention despite many challenges such as the high specific power requirement (about 2~4 kW/kg or higher for civil turbofan engines [6]) and the high specific energy requirement for energy storage system (jet fuel has a specific energy of 43 MJ/kg which is 30–40 times greater than that of the best batteries available [7]). Some attempts have already been made to demonstrate the great potential of using electric machines to provide thrust force for aircraft first on unmanned vehicles. In the late 1970s and early 1980s, the AeroVironment developed a solar-powered unmanned aircraft named Pathfinder. Six electric motors, each capable

of producing 1.5 kW power are installed to spin the propellers which are powered by solar arrays.

In 2014, Airbus revealed an all-electric aircraft (AEA) with two seats named E-fan which is shown in Figure 2 at the Berlin Air Show. The aircraft is equipped with two ducted fans powered by two electric motors, each providing 30 kW of power. Electricity is stored with a series of 250 V lithium-ion polymer battery packs which enables the aircraft to fly for an hour. The specific power of the is around 2.5 kW/kg and the overall efficiency is approximately 94% at the rated speed of 2500 r/min [8].

Figure 2. E-fan developed by Airbus.

Both of the aircraft mentioned above adopted the all-electric configuration as described in Figure 3. However, due to the limited specific energy of the battery pack, such a configuration becomes impossible for commercial airliners and military aircraft where a longer flight duration is needed. According to a study carried out by engineers from Pratt & Whitney, the state-of-the-art (SOA) battery energy density is still too far from practical use even when the specific power of the electrical system (including the cable, cooling, electric machines, power electronic devices, and other additional components) increases to 12 kW/kg for single-aisle airliners. Such difficulty can also be concluded

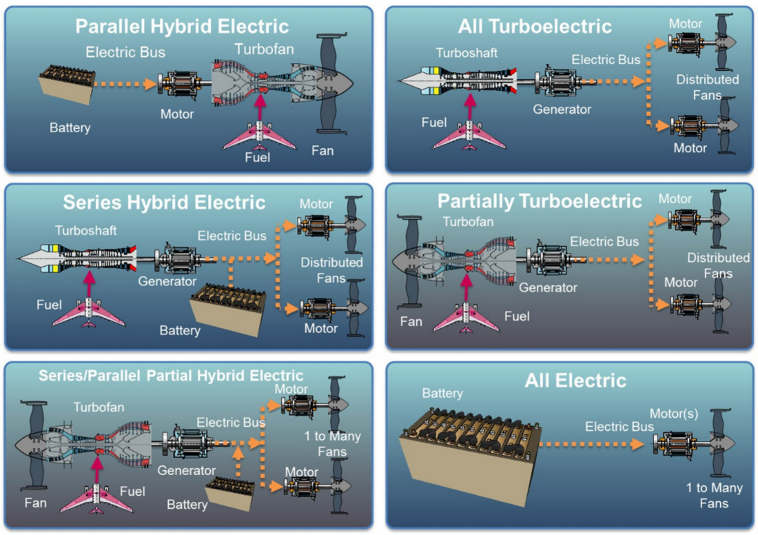

Figure 3. Classification of aircraft electric propulsion architectures [4].

Therefore just like what has been practiced in the car industry, many other alternative schemes that incorporate the high specific power fuel powered system with the highly efficient electric propulsion systems as shown in Figure 3 have been explored. As shown in Figure 3, except for the parallel hybrid electric propulsion configuration, the thrust force comes solely or partially from motor-driven fans in hybrid propulsion systems. In other cases where turbofan engines are used, the jet engine can also provide a certain amount of thrust force for the aircraft. Among all the hybrid configurations, all turboelectric and partially turboelectric configurations have been viewed as the most promising approach to

reducing carbon emissions of commercial airliners at present mainly due to the possibility of minimizing or even eliminating the weight of battery and fuel cells [9]. In the turboelectric configurations, the battery packs are freed from the responsibility of providing the major power to the propulsion motors and are used as power buffers only therefore their weight can be reduced. Combined with boundary layer ingestion (BLI) techniques and distributed propulsion configuration where multiple electric drive units are used, fuel consumption is expected to be reduced by 20% [10].

NASA developed a Single-aisle Turboelectric Aircraft with a rear Boundary-Layer propulsor or "STARC-ABL" which adopted the partially turboelectric configuration in 2017. Two generators are attached to the two turbo-fan engines with reduced size to power the additional fan at the rear of the aircraft. The specific power of the electric machines is approximately 13.15 kW/kg and that of the inverter is higher than 16.4 kW/kg. 1000 Volt high voltage electric system is used to reduce the weight of the electricity distribution system and the transmission loss when supplying power from the two 1.4 MW generators to the 2.6 MW rear motor [11]. With this hybrid electric configuration, fuel consumption is predicted to be reduced by 10%.

In 2022, Honeywell tested a turbo-generator capable of producing 900 kW of electricity continuously and 1 MW at peak. The overall weight of the generators is 127 kg featuring a high-power density (~8 kW/kg) and efficiency (~97%) and is merely 60 × 35.6 cm in size. The generator can either be integrated into the current APU system to reduce the weight of the unit or to provide power for multiple traction motors.

In 2023, researchers from MIT unveiled a megawatt-class motor drive demonstrator which is believed as a key enabler for large-scale aircraft to achieve net-zero emission goals. The motor drive is shown in Figure 4 featuring the integration between the high-speed permanent magnet synchronous machine (PMSM) and the power electronics by which a shared cooling system is enabled. With all the components including the cooling system, the specific power of the motor drive is estimated at 10.5 kW/kg [12].

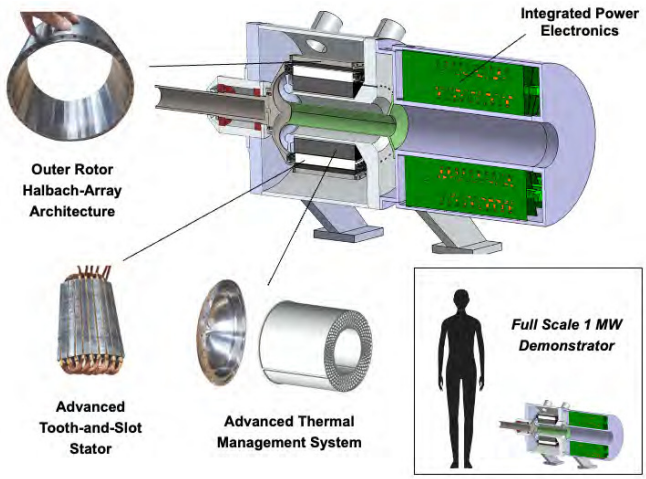

Figure 4. Full-scale 1 MW motor drive demonstrator for turbo-electric propulsion developed by MIT [12].

A bolder solution to overcome the insufficient battery energy density while satisfying the net zero carbon emission goal is to take advantage of the liquid hydrogen (LH_2) due to its attractive gravimetric energy density (143 MJ/kg, which is over three times that of jet fuel) and the zero CO_2 emission characteristic during the flight [13]. Hydrogen can be used either in fuel cells or in turbine engines to replace fossil fuels.

Some modifications have been made to the jet engine system to allow the effective combustion of hydrogen and control the flaming temperature to avoid NOx emissions [14]. The first successful experimental demonstration of using liquid hydrogen as fuel in the turbofan engine was made by the Tupolev on Tu-155 in 1988 [15]. Later during 1995–2000,

Lockheed carried out a study to evaluate the possibility of using LH_2 considering factors such as the airport requirement, the distribution and transport of LH_2, the storage approach, and the liquefaction process. It is concluded that using LH_2 as aviation fuel is feasible with more advancements made to reduce the cost and the risk during the entire lifecycle [16]. According to [17], polymer electrolyte membrane fuel cells (PEMFC) have the highest power density compared with other types of fuel cells. The LH_2 stored in the cryogenic hydrogen tank and oxygen in the air are combined electrochemically across a membrane that only conducts protons. Meanwhile, the electrons that break off from the hydrogen molecule will flow through the external circuit, supplying electricity to the motor drive unit [18]. During the process, electricity, water, and heat are generated. The overall energy efficiency of PEMFC can be as high as 45~60% which can be further increased when the wasted heat can be effectively recovered [19]. Despite the attractive advantages, both solutions mentioned above face mutual challenges, including the cost-effective production and liquefaction of hydrogen, safely storing and transporting hydrogen without significantly increasing the weight and drag force of the aircraft, and reducing CO_2 emissions during the production, transport, and liquefaction processes.

In summary, electric motor and generator systems are essential in aircraft regardless of the specific aircraft configuration. Considering both the MEA and AEA trends, the functions of electric machines include driving actuators, fuel pumps, high-speed compressors, acting as starters/generators attached to gas turbine engines, and driving propeller fans. While the focus and design priorities of electric machines vary depending on the specific application, systems with higher power/torque density, greater efficiency, improved fault-tolerant capability, and enhanced robustness in harsh environments are consistently sought after across all aeronautic applications.

In the following context, the most viable technological approaches towards the development of more/all-electric commercial airliners, which are considered one of the most significant contributors to greenhouse gas emissions, are discussed from the perspective of electric machine design. The important roles and targeting applications of electric machines in the aeronautic field are highlighted in Section 1. A brief introduction and characterization of the permanent magnet (PM) machines is provided in Section 2. In Section 3, key design considerations of PMSM design for different functions are discussed. Next, in Section 4, advanced and promising techniques to improve the performance of aeronautic PM machines are discussed and reviewed.

2. Characteristics and Topologies of PM Machines

Due to the special working conditions of aeronautic applications, reducing the weight and the volume of the electric drive system has always been a necessity to save more energy. Among various electric machine topologies, machines with permanent magnets therefore are preferred in most aeronautical motoring situations due to the following reasons:

First of all, the implementation of high-product energy PMs allows for low excitation loss compared with electrically excited counterparts [20] such as induction machines, wound rotor machines and switch reluctance machines. This feature not only improves the overall efficiency but also simplifies the thermal management of the system because excitation winding overheat will no longer be a risk.

Secondly, the PMs can generate a strong excitation field within a limited volume and weight, making it possible to provide sufficient torque under strict weight and space limitations [21,22].

Lastly, adopting PMs in electric machines can eliminate the conventional carbon brush and commutator structure which is mechanically unstable when exposed to an environment where significant temperature variation and strong vibration [23]. Both the maintenance cost and the sparking risk [24] can be reduced when sliding contact components are eliminated.

Based on the back electromotive force (back-EMF) waveform of the permanent magnet machines, they can be categorized as PM sinusoidal AC machines and PM trapezoidal AC

machines as stated in [25]. Typically, PM sinusoidal AC machines are preferable in high-performance motoring applications since smooth torque can be generated when current harmonics are well-filtered. To generate sinusoidal phase current, pulse-wise modulation is needed where both accurate phase current sensors and a continuous high-resolution rotor position sensor are required to achieve the ideal smooth output torque performance. As a result, the electronic switches of the drive will have to turn on and off multiple times within one electrical period. The switching-to-fundamental frequency ratio should be high enough (typically should be higher than 10) to maintain a low current ripple at the cost of increased switching losses. On the contrary, the PM trapezoidal AC machines are less sensitive to the resolution of the rotor position sensor and only one current feedback sensor is needed since quasi-square-wave currents are employed. Therefore both the cost and the switching losses of the motor drive can be reduced. However, due to the higher flux density harmonic contents in the air gap, high core losses are expected when the rotating speed is high which can cancel the advantage of lower switching losses. Furthermore, the large commutation torque fluctuation of PM trapezoidal AC machines can cause higher noise and vibration when they are operating within a wide speed range.

Many PM synchronous machines (PMSM) topologies are designed to modify the flux density and the back electromotive force (back-EMF) waveforms as was partly shown in Figure 5. Arrows are used in the figure to indicate the magnetization direction. Depending on where the magnets are located, there are typically three types of PM machines, namely the interior type, the insert type, and the surface type. The rotor with PM can be either on the outer side of the machine or the inner side or as in some cases, the rotor with PM and the stator are unrolled and arranged in parallel, the construction remains almost the same as indicated in Figure 5d.

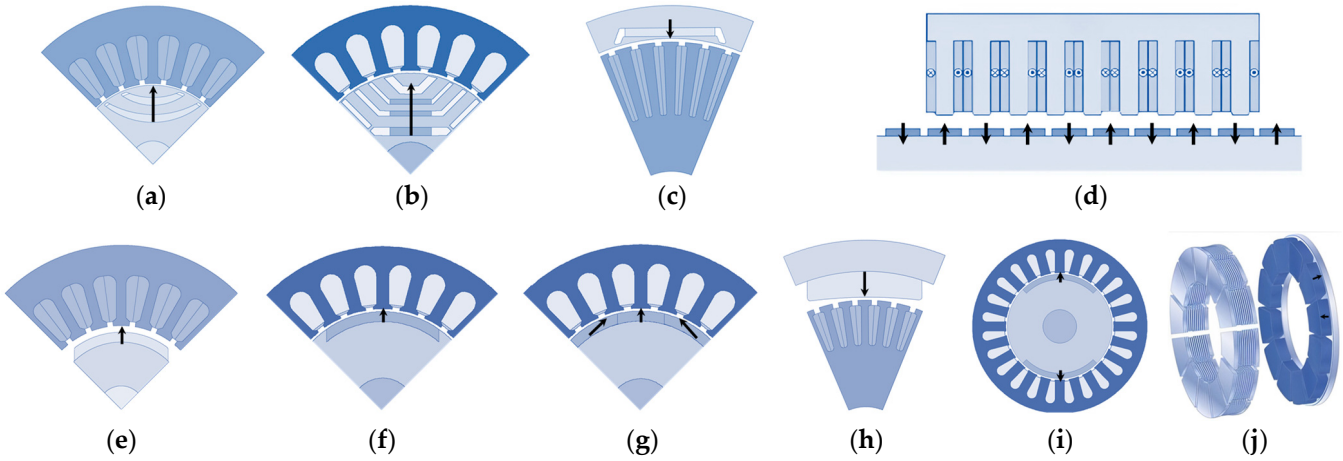

Figure 5. Different PMSM topologies (**a**) interior PM (**b**) PM-assisted synchronous reluctance (**c**) interior PM outer rotor (OR) (**d**) surface-mounted PM linear (**e**) surface-mounted PM (**f**) surface-inset PM (**g**) surface-mounted Halbach PM array (**h**) surface-mounted PM OR (**i**) consequent pole surface-inset PM (**j**) surface-mounted PM axial flux.

In interior permanent magnet (IPM) machines, the PMs are installed in pockets within the rotor laminations. In this case, the reluctance torque caused by these pockets in the rotor laminations, along with the PM torque generated by the PM field, are responsible for torque production. When the magnet pieces are partially removed from the IPM machines as shown in Figure 5b, the contribution of reluctance torque to the overall torque further increases, leading to the possibility of saving more PM materials and better flux weakening ability. For this reason, the IPM and PM-assisted synchronous reluctance machines have become very popular in many civil applications that are sensitive to cost such as electric vehicles [26–28], home appliances [29,30], etc.

However, since the PMs are buried inside the magnetic steels, it is crucial to maintain a short air gap length to limit the stray PM flux. The lower airgap length makes the machine more sensitive to eccentricity and core saturation due to armature reaction which can lead to high torque ripple, making them less attractive in aeronautical applications. The nonlinearity behavior caused by the saturation effect increases the complexity of motor control as well since the optimal *d*- and *q*-axis current are closely dependent on the operating condition. Another disadvantage is that the thin magnetic bridge aiming to limit PM leakage flux on the rotor lamination cannot withstand high mechanical stress, making the maximum rotor linear velocity difficult to exceed 160 m/s, as indicated in Figure 6.

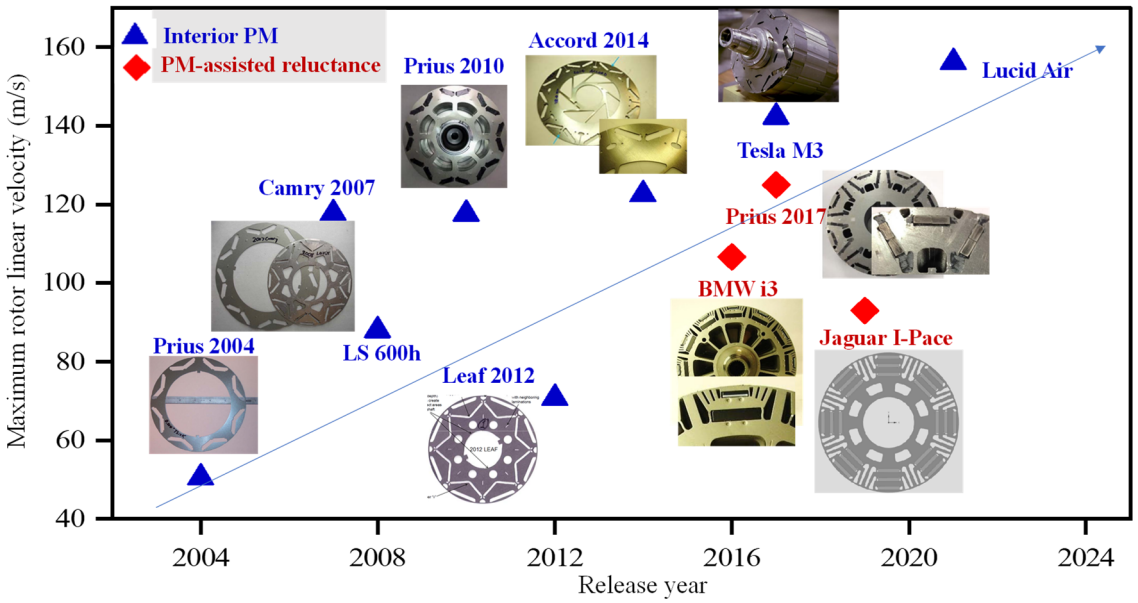

Figure 6. Maximum rotor linear velocity of PM motors for electric vehicles [31–40].

A comparison between various PMSM topologies is presented in Table 2. The surface-mounted permanent magnet (SPM) machines and surface-inset permanent magnet (SIPM) machines are very similar, both of which feature PMs that are exposed to the air gap and a retaining sleeve for the protection of magnets. The main difference is that the PMs in SIPM machines are installed in the notches on the outer surface of the rotor laminations rather than directly attached to the outer surface of the rotor, making it possible for them to utilize the reluctance torque just like the IPM machine did. However, due to the existence of a non-magnetic rotor sleeve, the contribution of reluctance torque to the total torque will be reduced.

Reducing the pole-arc length of the magnets in SIPM machines shown in Figure 5f and keeping all the PMs magnetized uniformly either inward or outward, a SIPM machine with the consequent pole is constructed. As indicated in Figure 5i, the consequent pole PM machine reduces the PM usage by half by using the inter-PM rotor iron as the equivalent magnet pole (south pole in Figure 5i). However, due to the artificial magnet pole, significant flux density harmonics (including even order harmonics) will be generated leading to higher core losses, torque ripple, and lower torque density.

The SPM machines have become more popular in aeronautic applications rather than IPM machines for several reasons:

1. Capability of operating at high speed with the help of high-strength retaining sleeves which enables them to be directly coupled to high-speed turbines and compressors.
2. Higher power density and faster dynamic response can be achieved when more PM materials are used [41,42] since the cost of magnets is not the priority in aeronautic applications [43]. When an optimized coreless Halbach array rotor is used, intensified

air gap flux density [44], reduced rotor yoke thickness, and low flux harmonics can be achieved simultaneously.

3. A lower torque ripple can be expected [45] since SPM machines are less sensitive to the slotting effect and saturation caused by the armature reaction.

Table 2. Comparison of different PMSM topologies.

PMSM Topology	Key Features	Reluctance Torque Contribution	Inter-Pole Flux Leakage	Airgap Flux Harmonic
Interior PM	Thin magnetic bridges	High	Low	Low
PM-assisted synchronous reluctance	Low PM usage	Very High	Low	Low
Surface-mounted PM	Thick retaining sleeve	None	Low	Medium
Surface-inset PM	Rotor slot for magnets	Medium	High	Medium
Surface-mounted Halbach PM array	Multiple PM segments per pole	None	Low	Very low
Consequent pole	Asymmetrical poles	*	Low	Very high

* Consequent pole PMSM can be either interior type, surface-mounted type, or surface-inset type; therefore, the contribution of reluctance torque will be dependent on the specific configuration.

Although the radial-flux machines have dominant popularity, axial flux machines as shown in Figure 5j have received growing attention recently due to their high volumetric torque density when operating speed [46] and low diameter-to-axial-length ratio (less than 0.3) is low [47]. These features make them an attractive candidate for low-speed aircraft applications such as direct-drive electric propulsors. However, the axial force increases can drastically increase due to nonuniform airgap length caused by eccentricity, vibration, and thermal expansions [48] which increases the risk of mechanical failure such as bearing fault. Additionally, they are more difficult to manufacture with conventional techniques especially when complex sandwich structures are adopted [49]. Many research efforts have therefore been conducted to reduce the fabrication complexity and improve the mechanical reliability of axial-flux machines, which will be discussed later.

So far, aeronautic PM synchronous machines have mostly been used as motors and are seldom used as generators mainly due to the difficulty in adjusting the powerful PM field. Unlike in motoring mode, the power source which is often the engine shaft cannot be immediately shut down when in power generation mode. This can bring the risk of severe overheating and destruction to not only the machine system itself but also the entire onboard electrical system when a short-circuit fault occurs. To incorporate the benefit of a brushless PM machine and avoid the aforementioned risks, many other PM machines featuring both PM excitation and electrical excitation have been explored.

An additional axial flux generated by the DC field winding in the end plate is introduced in [50] as a controlled flux shunt, enabling the regulation of flux in the radial air gap. The configuration of the flux paths are presented in Figure 7 in which the yellow block indicate the magnet. During the experimental tests, the air gap flux density was successfully regulated within a range of 0.21 T to 0.86 T, demonstrating the feasibility of maintaining a steady output voltage across a wide range of speeds and load variations.

In [51], different hybrid-excitation machine topologies are compared. These topologies can be mainly categorized as serial hybrid and parallel hybrid. It is concluded that the serial type has weaker flux regulation ability due to the additional air gap introduced by the magnets. Detailed discussion about the design considerations are presented in [52]. With proper selection of the length combination of the PM section and the wound field section, a constant voltage can be obtained utilizing the bi-directional adjusting capability enabled by the DC field windings. In the event of a short circuit fault, the DC field current can be adjusted to counteract the flux generated by the PMs, effectively limiting the short circuit current in the armature.

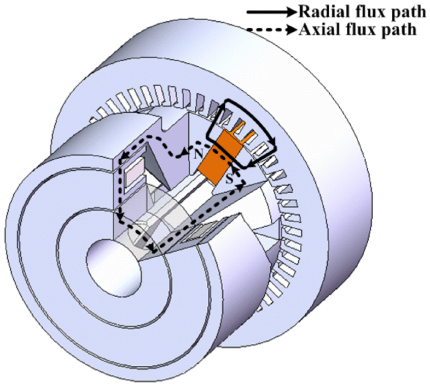

Figure 7. Radial-axial magnetic flux path in hybrid excited PM machine [50].

Similarly in [53], a hybrid-excitation flux switching (HEFS) DC generator is designed. The no-load flux is created on the stator side by both the PMs and excitation coils. The magnetic flux generated by these two sources is connected in parallel, the intensity of the air gap flux can then be easily regulated when the engine shaft speed changes by adjusting the DC that flows in the excitation coils. Since no further regulation is needed to maintain a constant voltage, a reliable diode bridge rectifier will be sufficient. Compared with conventional flux-switching machines, the magnets in HEFS are shorter, leaving room for excitation coils [54]. This parallel excitation configuration is preferable compared with the serial excitation type not only because of the increased flux regulation capability but also due to reduced demagnetization risks since flux generated by excitation coils does not directly go through the PMs.

All the hybrid-excited machines mentioned above adopted the doubly salient structure to achieve brushless excitation. Since both windings and PMs are located on the stator, it is easier to dissipate the heat of these parts. The introduction of excitation coils and the weakened role of the PMs increases the flexibility of voltage regulation over a wide-speed range which can be attractive in onboard generation applications. However, the high torque and speed fluctuation due to the salient pole structure and core saturation limited their application in motor applications [55]. The additional DC power source and regulator further reduce the overall power density. The excitation coils not only increase the overall copper loss but also complicate the generator system leading to a potentially higher possibility of fault.

3. Key Design Considerations of PM Machines in Aeronautics Application

3.1. Actuators

Using electric motor-driven actuators to replace conventional hydraulic and pneumatic actuators can get rid of the heavy fluid transmission system that extracts power from the engine [56]. As a result, both the maintenance cost and the weight of the power transmission system (pipelines, ducts, and heat exchangers) can be reduced. Meanwhile, the energy efficiency of the aircraft will be increased thanks to the high-efficiency electric drive system (typically above 95%). Currently, electro-hydraulic actuators (EHA) are preferable to electro-mechanical actuators (EMA) mainly due to the risk of mechanical jamming of the gearbox or ball screw as indicated in Figure 8. But EMAs make it possible to delete the hydraulic pump therefore less maintenance and weight can be achieved [57]. Nevertheless, although the power ratings and load profiles of different actuators are very different depending on the function and the aircraft [58], there are still some common design principles that need to be followed.

Actuators on aircraft are often used in some of the most critical situations such as adjusting the flight surface, the landing gears, and cargo doors. Therefore it is important that these electric motors can respond to the command signal rapidly and can be controlled with satisfying precision. Additionally, they are often installed within very limited space where extreme temperatures and strong vibrations can occur. The working temperature

mostly varies from −40 to 77 °C [59], in special occasions where the actuator is used in an engine, the working temperature can reach 125 °C [8].

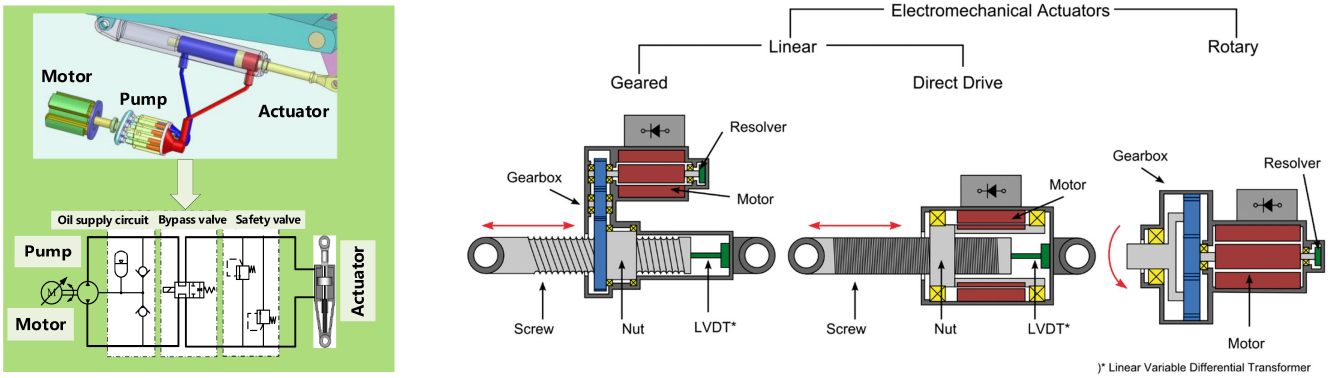

(**a**) (**b**)

Figure 8. Structure of electric-driven actuators (**a**) EHA [60] (**b**) EMA [57].

Therefore, the focus of designing the electric motor implemented in electric-driven actuators for aircraft should be to improve the response speed and fault tolerance ability, decrease the torque ripple, and improve the torque density and overall efficiency [61].

In [62], a PM brushless motor is selected as the driving machine in an electro-mechanical actuation system. Two different machine configurations: 3-phase, 6-pole, 9-slot, and 6-phase, 10-pole, 12-slot are considered and compared. It is found that using cobalt steel instead of silicon steel can effectively improve power density and reduce rotor inertia. Another approach to decrease rotor inertia is to increase the operating speed of the motor. As the motor speed increases (typically from 1500 to 15,000 r/min) [63], the volume of copper, magnets, and laminations will decrease. However, in the actuation system, the performance relies not only on the dynamic response of the motor but also on other mechanical and hydraulic components. Therefore the motor speed and the gear ratio of the reducer should all be taken into consideration when designing an electric motor-driven actuator [64,65]. But from the standpoint of eliminating mechanical jamming faults, the direct drive solution with optimized motor configurations seems to be more advantageous due to the flexibility of motor optimization [66]. Also to reduce the risk of failure, samarium cobalt magnets are often used due to their thermal compatibility and low temperature coefficients. It is found in [67] that the back-EMF reduces only by 2.57% when the temperature increases from 20 °C to 150 °C which can easily be compensated by slightly increasing the phase current.

To further improve the stability and reliability of the machine, the fractional slot concentrated winding (FSCW) configuration with multi-phases has become a popular option. FSCW can effectively reduce the height of end windings which is beneficial to loss reduction and compactness of the system. In [68], a FSCW five-phase PM machine is designed for aircraft flap actuation. Since it is emphasized that these machines must operate safely even when phase winding-related faults occur, single-layer windings are adopted to prevent windings belonging to different phases from overlapping [69]. Thermal isolation and low mutual inductance can be achieved as well [70,71]. The experimental results demonstrate the capability of producing rated torque when one or two phases are out of function by increasing the phase current of the healthy phase.

3.2. Fuel Pumps

Similar to the actuator application, electric motors used to drive the fuel pump are also expected to continue to provide rated torque in case of single-event machine failure [72] so that the engine can continue to operate. In [73], a detailed introduction and rotor losses analysis of a four-phase single-layer FSCW motor is presented. Surface-mounted Halbach PM array is implemented to minimize the magnetic flux density harmonics in the airgap. Still, the PM and sleeve eddy current losses are identified as one of the most dominant

losses in the machine due to the abundant magnetomotive force harmonics inherited by the FSCW machines. Measurements such as asymmetrical tooth design and modifying airgap length have been considered to tackle this problem. Regarding copper losses, Litz wire can be used to mitigate the AC effect, allowing for an increase in the fundamental frequency without raising the risk of thermal failure in the insulation. To further improve the fault-tolerant capability of the pump-driven motor, the dual-winding six-phase configuration is adopted in [74]. In the event of an open circuit fault or short circuit fault in phase windings, the faulty channel will be removed and the healthy channel will increase its power to compensate for the power loss. Despite the increased post-fault operating capability, the system's power density is compromised as a trade-off.

One good compromise between the system power density and the post-fault operating capability would be to increase the thermal performance of each channel rather than adding redundant channels. Unlike those used in actuators that only work at command, the pump-driven motor works during the entire flight, therefore the thermal management is of greater importance.

Since the aircraft fuel is quite accessible for pump-driven motors, it can be considered an ideal cooling agent. In [75], the entire motor is immersed in fuel for cooling purposes to increase the available current density. Experimental test results show that the immersed liquid cooling configuration can effectively ensure a modest temperature rise even under faulted conditions. Liquid cooling ducts have been integrated into the stator yoke, stator slot openings, between the flat wires in the slot, and along the outer radius of the stator core to further enhance heat dissipation capabilities [76]. With the enhanced configuration, the temperatures of critical components, including the windings and magnets, are effectively maintained within their thermal limits.

3.3. High-Speed Air Compressor

Unlike pumps and actuators, the speed requirements of motors for air compressors are much higher to enable a direct coupling scheme. For example, the PMSM used to provide pressurized cabin air in Boeing-787 operates at 22,000~44,000 r/min with a rated power of 100 kW (rotor surface speed exceeds 144 m/s). The maximum speed of the 40 kW motor used in the nitrogen generation system can even reach 80,000 r/min. Besides the fault-tolerant capability, high power density, and low loss requirement, rotor mechanical strength and critical speed evaluation have become the most important design considerations of aeronautic high-speed motors.

As explained earlier, SPM machines are considered to be more suitable than their IPM counterparts. However, the thickness of retaining sleeves requires careful inspections. Thinner sleeves lead to higher torque and the potential of reducing rotor eddy current losses, yet might compromise the mechanical strength of the rotor due to the high centrifugal force at high speed. The sleeve can be either made of metallic alloy or carbon fiber. Metallic alloy generally has higher electric conductivity and thermal conductivity meaning that higher eddy current losses and better rotor heat dissipation capability can be expected. Generally, carbon fiber materials have much higher strength in the circumferential direction and lower mass density than most metallic materials [77–79] meaning that the sleeve thickness at a given condition can be minimized when a carbon fiber sleeve is adopted. As a result, the power density and the dynamic response of the high-speed motor can be enhanced. However, the carbon fiber has low strength in the radial direction which can be dangerous when local bending stress caused by magnet segmentation is considered [80,81]. Therefore materials that can withstand high bending stress such as glass fiber [80] and Ti-Alloy [82] can be used at the inner surface to protect the carbon fiber sleeve.

Apart from the mechanical aspect, rotor loss is another key issue in high-speed PMSMs for compressor-driven applications since air cooling is preferred instead of liquid cooling to prevent liquid leakage and complex cooling design. As demonstrated by the comparison in [83], although carbon fiber sleeve reduces the sleeve eddy current, the overall rotor eddy current losses get higher than those adopting metallic sleeves. This is because the

eddy current in metallic sleeves shields the airgap magnetic flux from entering PMs and rotor cores, leading to loss reduction within these components. A contradictory result is provided in [84] showing that a rotor with a carbon fiber sleeve exhibits less eddy current loss compared with the case where a stainless steel sleeve is used. Such difference can be explained by the different airgap flux harmonic compositions since the penetration depth of each flux harmonic is influenced by the operating speed, and the spatial and temporal order of the airgap flux harmonic [85,86]. Therefore, the optimal sleeve configuration is case-dependent. Since in-shaft liquid cooling is not available in this application, adopting a metallic sleeve or carbon fiber sleeve with metal shields [87] to concentrate the rotor eddy current loss to the rotor surface is a more reasonable design to make it easier to dissipate heat in the rotor. Combined with other techniques such as magnet segmentation [88–90] and stator slot optimization [91], the rotor losses can be further reduced to ensure the safety of the magnets.

The critical speed is another limiting factor in high-speed PMSMs. To avoid undesired rotor resonance completely, the first-order critical speed of the rotor should be kept at least 10% higher than the maximum operating speed [92]. This can be achieved by increasing the bearing stiffness, limiting the axial length of the end-windings, increasing the shaft stiffness by implementing new materials or increasing shaft diameter, reducing the additional mass by adopting PMs with higher remanence, etc. Besides, high-precision rotor balancing is also necessary to minimize the impact of the rotor resonance. As for the bearings, since no liquid cooling is allowed, non-contacting magnetic bearings [93] and airfoil bearings [94] are more suitable choices due to merits such as longevity and low friction loss instead of liquid lubricated mechanical bearings [95]. It should be mentioned that a longer airgap length is preferred when non-contacting bearings are used to prevent vibration and rotor displacement from causing severe mechanical damage. Finally, it should be emphasized that the rotor design of PMSMs for this application is a multi-physics optimization problem including electromagnetic analysis, thermal analysis, mechanical analysis, and modal analysis [96,97]. More effective design approaches must be explored to better facilitate the optimization of the motor [98–100].

3.4. Engine Starter and Power Generation

Although much research has been carried out to explore the possibility of implementing the PM starter-generator (PMSG) in the aircraft generation system, the three-stage wound-field synchronous machines shown in Figure 9 are still the dominant machine types in this application. Rotors of each stage are installed in one common shaft which is connected to the engine shaft through an accessory gearbox as indicated in Figure 10. When it is operating in generation mode, the rotating magnets will cause three-phase AC in the stator windings of the PM generator (PMG) which will then be rectified to controllable a DC. The DC is then supplied to the stator winding of the main exciter (ME). The induced AC on the rotor coils of ME is rectified to DC by the rotating rectifier and then serves as the field current of the main generator. Although power generation is the major function of the machine, utilizing it to drive the engine shaft to a required speed instead of relying on external compressed air suppliers can be seen as a crucial improvement to simplify the operation of the aircraft. When trying to start the engine, the PMG is open-circuited. AC is fed to the stator windings of ME which will then induce current on the rotor windings of ME. Then, the rotating rectifier will convert the AC to DC to excite the main generator. Once varying frequency AC is fed to the stator windings of the main generator, starting torque can be generated and now the machine will be working in motoring mode [101].

According to the descriptions above, the main limitation of this three-stage SG can be concluded as follows:

- The rotating rectifier is unable to withstand the centrifugal force caused by high rotating speed, prohibiting the SG from direct coupling to the engine shaft.
- The complex control strategies and the additional AC power sources needed during the starting mode increase the risk of electrical fault and reduce the overall compactness.

- Windings and rotating rectifier on the rotor lead to significant rotor losses which can be difficult to dissipate, posing as a major threat to the operating safety [102].

PMSGs featuring negligible rotor losses on the other hand can operate at high speed and produce higher power within in confined volume, showing promising potential for replacing the three-stage SGs. Furthermore, attaching the PMSG rotor directly to the engine shaft or increasing the PMSG speed with the current configuration makes it possible to minimize or even eliminate the accessory gearbox. This reduction in mechanical components leads to decreased aerodynamic drag and takeoff weight, contributing to overall aircraft efficiency [103,104]. However, the demagnetization risk and the challenges of managing short circuit currents have been the primary factors limiting the adoption of permanent magnet synchronous generators (PMSGs) in aircraft applications.

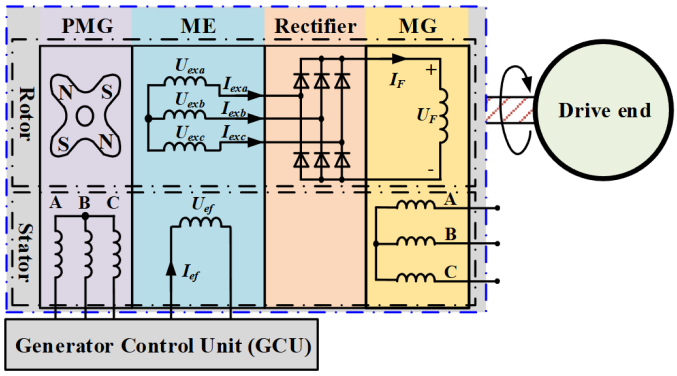

Figure 9. The architecture of the three-stage wound-field synchronous SG.

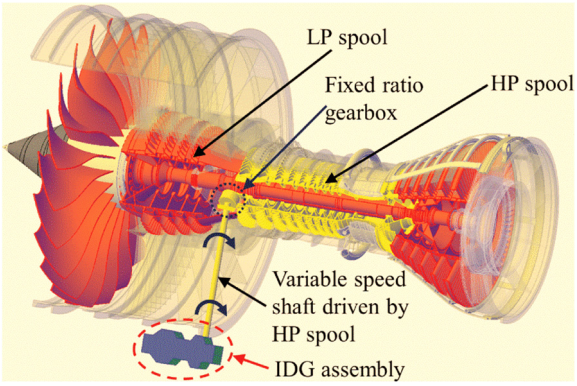

Figure 10. Typical dual-spool turbofan engine with integrated drive generator (IDG) [105].

To limit the impact of short circuit current, improving the reactance of PMSGs has been considered an effective approach because no additional hardware as presented in [106,107] is needed. This can be achieved in several ways, such as increasing the slot leakage inductance through designs like deep narrow slots [108], auxiliary tooth [109], and closed slot [110], or by enhancing harmonic leakage inductance and self-inductance using FSCW configuration [111]. However, the increase in leakage inductance will inevitably compromise the power density. Instead of increasing the leakage reactance, some researchers adopted the multi-channel configuration to minimize the impact of short circuit current. As described in [112], a negative d-axis current will be injected into the healthy set of windings in the dual-three-phase PMSM to weaken the PM field, thereby limiting the short circuit current in the faulty windings. As a result, the output power will be reduced to less than 50% of the rated power. Besides, since the armature field flux is in series with the PM field flux, a high demagnetizing ampere-turn number is expected, which increases the risk of excessive magnet eddy current loss and demagnetization when a short circuit happens.

Alternatively, reducing the flux linkage provided by the PM and substituting them with those generated by the field windings has been a popular option. This can be done by configurations introduced earlier such as hybrid-excited doubly salient machines and hybrid-excited flux switching machines. In the event of a winding short circuit fault, the current in the electrically excited field windings can be adjusted to zero or even set to a negative value to counteract the PM flux linkage. This approach effectively limits the short circuit current to a manageable range, which the cooling system can handle efficiently. In [113], experiments showed that the short circuit current is only one-half of the rated current even without the canceling effect of the electrical excitation part. The hybrid-excited doubly salient machine presented in [114] provides near-zero flux linkage when the field current I_f is set to zero and ten times the flux linkage at the rated I_f. This demonstrates its potential for fault tolerance and high starting torque. Fault tolerance of SGs can also be achieved at the system level, as illustrated in Figure 1, where two electrically and magnetically isolated SGs are attached to each of the two engines, with additional two SGs installed in the APU.

The main challenges with hybrid-excited machines are their reduced power density and the need to limit the electrical air gap length. If the airgap length is not properly managed, the excitation efficiency of the electrical excitation system will significantly decrease, leading to an even lower overall power density. Typically, the airgap length of the electrically excited flux path can be limited to 0.2~0.5 mm [115–120] which can increase the risk of mechanical failure considering factors such as the mechanical stress due to centrifugal force, thermal expansion, and engine-induced vibration as indicated by Figure 11. Such mechanical difficulty can be even more severe when the SG rotor is attached to the high-pressure turbine shaft with a sizable outer radius and high ambient temperature. Considering the limited radial space available and the high power density requirements, fault-tolerant SPM SGs with a longer physical airgap length seem to be the only reasonable solution. Many design principles introduced earlier such as single-layer FSCW, multi-phase arrangements, and temperature-resilient magnets can also be implemented in this case. Advanced liquid cooling techniques such as direct winding cooling and hollow shaft liquid cooling using the fuel can be necessary to ensure the safety of the SGs.

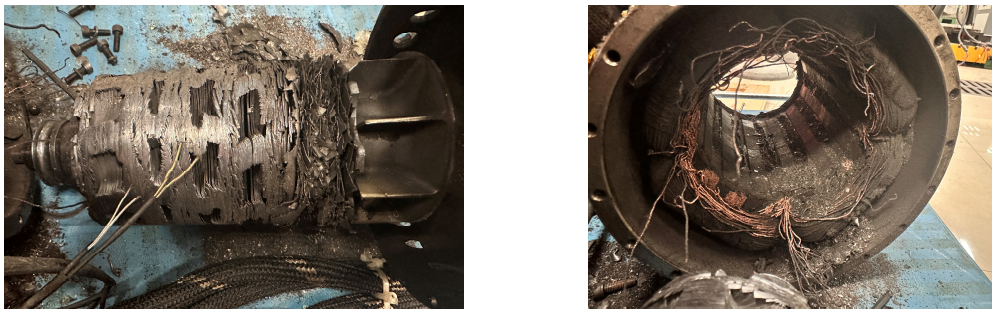

(**a**) (**b**)

Figure 11. Mechanically failed doubly-salient SG (airgap length = 0.7 mm) (**a**) rotor (**b**) stator.

3.5. Electric Propulsion

As mentioned earlier, the turboelectric configuration is by far the most likely solution for developing electric propulsion to significantly reduce aviation carbon emissions. In such configurations, mainly two functions are required from electric machines: generating power for traction motors and driving the propellers.

Because adopting two large-scale engines provides optimal combustion efficiency and minimal fault-tolerant ability, the desired output power of the generator in a turboelectric propulsion system is much higher than those used as SGs in MEAs which can be as high as 1~22 MW or even higher depending on the size of aircraft [10,121]. Similar to SGs in modern MEA, these generators are also required to be self-fault-tolerant, capable of withstanding high temperatures and vibrations, and immune to the impacts of short-circuit

currents. Considering their high power rating, the improvement of power density will bring a significant weight reduction. Therefore measures such as increasing the rotor speed and number of poles (less yoke thickness and shorter end-windings span), the overall efficiency (less thermal burden), and the voltage level of the onboard power system become even more urgent.

In [122], a 4-MW 8-three-phase SPM liquid-cooled generator is designed and tested. Many techniques introduced earlier have been used as well such as the Halbach magnet array (for eliminating rotor back iron and PM spatial flux density harmonics [81]), in-slot liquid cooling, high-performance SmCo magnet and CoFe as the stator core material. Litz wire insulated by Nomex is used to prevent excessive AC copper losses. The DC-link voltage is increased to 3 kV to reduce the rated current and copper weight, which is achieved through the series connection of two three-level converters. Within each of the independently controlled dual-channel, 4-three phase windings are connected with an independent converter in a series-parallel fashion. An additional control algorithm is implemented to balance the voltage of each converter to prevent circulating current and increase the longevity of the entire system. This configuration has stronger fault-tolerant capability compared with a 2-three phase configuration. It should be mentioned that with the bi-directional converter adopted, this generator can also serve as the starter of the turbo engine to avoid turbo lag.

As for the design of electric motors for propulsion, the OR configuration becomes more advantageous when they are directly coupled to the propeller since the rotating speed is limited by the diameter of the propeller. The typical speed of a direct drive propulsion motor can be 2000~4000 r/min [123,124]. In [125], a 20-pole OR SPM machine with a rated speed of 18,000 r/min is designed. To prevent the impact of high operating frequency, a toothless stator is adopted to reduce the stator core losses and reduce weight. Design parameters such as the PM thickness, stator yoke thickness, copper depth, and size of Litz wire are considered with the power density as the objective. Compared with the inner rotor configuration, a thick rotor retaining sleeve is no longer necessary in the OR configuration which is beneficial to the improvement of power density. Additionally, the OR configuration provides more space for accommodating PMs within a constrained volume due to the rotor's larger diameter compared to the stator, allowing for further reduction in axial length. The main disadvantages of OR configuration are the difficulty of dissipating the heat on the inner stator and increased mechanical vibration due to the cantilevered rotor. As a result, high-precision rotor balancing and more efficient stator cooling are needed. In [123], three different design concepts were compared. In concept 1 design, a high-speed OR motor is coupled to the propeller through a gearbox. The other two concept designs adopted directly coupled motors. The comparison result demonstrated that concept 3 provides optimal efficiency and gravimetric overall power density (considering the gearbox). The direct-drive OR configuration is selected eventually as a tradeoff between motor performance and manufacturability [126]. Since the motor is generally far from the oil tank and oil pipes, air-cooling becomes the most reasonable option. Litz wire capable of withstanding 180 °C is selected to ensure winding safety given the limited cooling capacity and the non-superconducting coils. Since the rotor speed is low, it is reasonable to force the axial airflow through not only the inner surface of the stator core but also the air gap so that the magnet can be effectively cooled. The stator windings of the 2.6 MW motor are segmented into four parts to improve fault tolerance and reduce the current load on the power switches, with each powered by an independent drive.

Unlike in STARC-ABL where a single megawatt electric propulsor is used to reduce aerodynamic drag and only produce 1/3 of the thrust force during cruising, full turbo-electric architecture with 16 distributed electric propulsors to take advantage of the BLI technique is adopted in N3-X as indicated in Figure 12. Using multiple distributed electric motor to provide all the thrust force is considered to be more fuel-saving. This can be explained from two aspects: first, both the engine and the electric machines (generator and the motors) can be designed to operate in their high-efficiency speed range; secondly,

a much higher effective bypass ratio can be achieved if the ducted-fan configuration is implemented, as demonstrated in [127]. Additionally, the multi-propulsor configuration allows for inherent fault tolerance, allocation, and flight control flexibility, and provides additional optimization dimensions for thrust improvement [128]. A 360 kW PMSM is designed for this purpose in [129] where both in-slot liquid cooling and hybrid coils are adopted as shown in Figure 13. The combination of flat wire windings (FWW) at the slot bottom and the stranded round wire windings (SRWW) near the slot opening can serve as satisfying tradeoff between the effective slot fill factor and the AC copper losses.

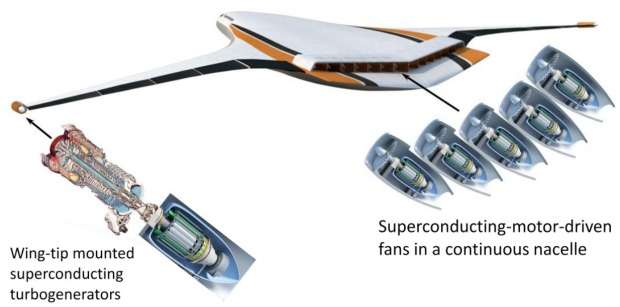

Figure 12. N3-X Aircraft with a Turboelectric Distributed Propulsion [130].

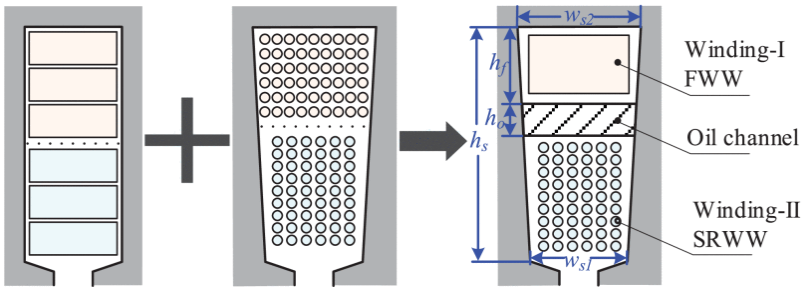

Figure 13. Evolution of the hybrid winding configuration [129].

To further reduce the copper losses and improve the current density, super-conducting coils are used in the turbo-generators and motors [131]. DC is fed to the rotor coils to generate a powerful rotating magnetic field instead of permanent magnets in these machines. The key to these superconducting machines will be effective lightweight cryocoolers and mitigation of AC losses. On-board LH_2 used in a hybrid electric propulsion system combined with hollow conductors can be an attractive approach for cooling superconductors to −252.87 °C, enabling a current density of 1780 A/mm^2 to be achieved using the MgB_2 wire [121,132]. On the stator side, a thin superconductor will have to be twisted to reduce the AC losses which increases the cost and fabrication difficulty. In the event of a short-circuit fault, the field current can be mitigated immediately by transforming the coil from a superconducting state to a resistive state or implementing a breaker [133]. To ensure the machine can continue producing electromagnetic torque in case of superconductor failure, NdFeB magnets are positioned next to the superconductors on the rotor as a backup exciter, as there is no risk of demagnetization at such low temperatures [134]. With advancements in new techniques, the cost of large-scale production and transportation of LH_2 is expected to decrease. As a result, it may be feasible to develop hybrid electric propulsion systems for long-range airliners, incorporating two or more superconducting or partially superconducting generators and multiple high-efficiency, lightweight electric propulsors in the future.

4. Emerging Techniques and Enablers of High-Performance PM Machines

Although many successful demonstrations and applications have already been made, the pursuit of electric machines with higher power density and higher efficiency is never-

ending. In this section, some of the most important enablers that can expand the limited capability of PM machines are discussed.

4.1. Materials

4.1.1. Electromagnetic Materials

Typical electromagnetic materials in modern aeronautic PM machines include SmCo (sometimes NdFeB with good cooling conditions) magnets, copper coils, and FeCo-based lamination steels. The selection of these materials is generally based on the principles of robustness in harsh environments and reduced overall weight, which also guides the development of new materials.

For PM materials, although NdFeB generally has a higher energy product than SmCo at room temperature, its high sensitivity to temperature rise makes it less powerful and more vulnerable to demagnetization risk as shown in Figure 14. As shown in Table 3, the reduction in residual induction and coercivity of NdFeB magnets is 3–4 times greater than that of SmCo magnets. The thermal stability of NdFeB magnets can be enhanced by adding rare earth elements like Dysprosium and Terbium, enabling operation at 200 °C. However, this significantly increases the cost, making it comparable to that of SmCo magnets. Considering the harsh operating conditions and high loss density in aeronautic PMSMs, SmCo materials are preferred for safety and reliability reasons. Optimization in terms of the chemistry and manufacturing process has been made by PM producers to further improve the energy product and thermal stability of modern Sm_2C_{O17} material. The most powerful Sm_2Co_{17} developed by Arnold can produce remanence higher than 1.2 T with the maximum energy product at the limit of this system of 34 MGOe [135].

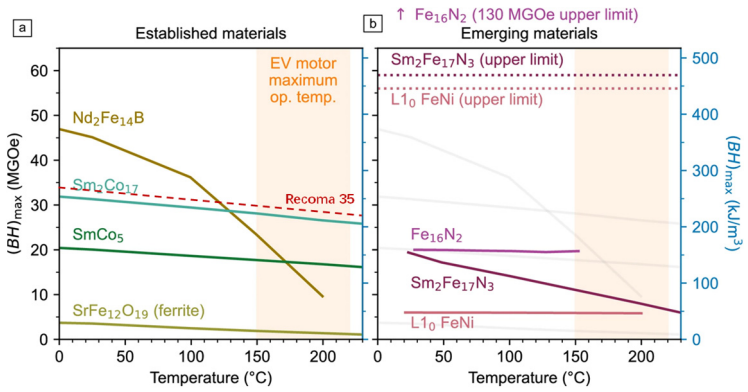

Figure 14. Temperature dependence of (BH)max for (**a**) established permanent magnet (PM) materials compared with (**b**) emerging PM materials [136].

Table 3. Comparison of NdFeB magnets and SmCo magnets.

Material		N40EH	N52	Sm_2Co_{17}
Mass density [kg/m^3]		7600	7600	8300~8500
Average price [CNY/kg]		350	181	300~350
Curie temperature [°C]		310		800–850
Maximum working temperature [°C]		200	60	350
Temperature Coefficients	α, Residual Induction	−0.12	−0.12	−0.03
[%/°C]	B, Intrinsic Coercivity	−0.47	−0.62	−0.20

New nitride PM materials as shown in Figures 14 and 15 show low (comparable with Sm_2Co_{17}) or even positive temperature coercivity coefficient. Although an energy product of only 20 MGOe has been achieved in recent reports on iron nitride materials, it is predicted that with refined powder preparation and synthesis techniques, this new light material could achieve an energy product of 45 MGOe [137] and a high Curie temperature of 540 °C [138]. With these high-performance PM materials, PM machines can achieve high

power density by reducing not only their effective mass but also the mass of the cooling system. The potential for implementing PM machines in more hazardous applications, such as direct integration with turbine engines, can also be realized.

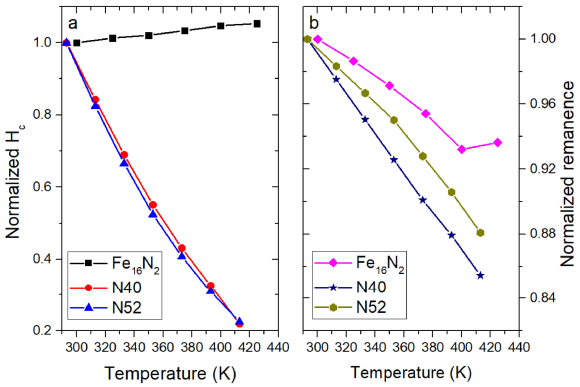

Figure 15. Temperature-dependent magnetic properties of $Fe_{16}N_2$ low-temperature nitride foil and NdFeB magnets N40 and N52 [139].

As for conductors, copper is widely used in electric machines as windings due to their superior electric conductivity and high ductility. Replacing them with silver which has slightly higher conductivity is not an option not only because of the cost but also the high mass density. Given the same resistance, using silver can increase the conductor mass by 10.75% at room temperature [140] which will deteriorate the power density of electric machines. Aluminum, however, can be considered a good alternative to copper since the conductor mass will reduce by 52% given the equal resistance despite the lower electrical conductivity. It is pointed out that in high-frequency applications, the advantage of the aluminum coils can be strengthened considering the AC effect [141]. Research in [142] shows that the difference in conductivity of these two materials reduces as the temperature gets lower. Electric conductivity of aluminum can even be higher than that of copper when ambient temperature gets below −195.25 °C which indicate that replacing copper with aluminum in high power density PM machines at low temperature may be beneficial. Considering the varying severity of AC effects in machine windings, partially replacing copper coils (such as those close to the slot opening) with aluminum coils appears to be an attractive way to reduce overall weight. Special connectors must be used to prevent erosion, and careful inductance calculations should be performed to achieve both low AC copper losses and reduced weight simultaneously. While quantitative criteria are challenging to establish, higher operating frequencies and lower ambient temperatures generally favor the use of aluminum or hybrid coils over copper.

An even lighter (mass density is 71% that of aluminum), highly conductive option is the carbon nanotube (CNT). Experiments in [143] showed that individual CNT is capable of sustaining a current density higher than 10^7 A/mm², which is over a thousand times that of copper, at 250 °C for two weeks without noticeable degradation. Since CNT coils are made from extremely thin sub-conductors meaning that they share the same benefit of Litz wire. A successful demonstration of a 3-slot 2-pole high-speed PM machine is presented in [144]. The tested conductivity of the CNT yarn conductor is 3.4×10^6 S/m which is much lower than that of copper due to the low purity of the nanotubes. Comparison in [145] showed that adopting CNT wire in a yokeless axial-flux PM machine results in lower gravimetric power density but increases volumetric power density, as more conductor cross-sectional area is required due to the assumed low conductivity. However, when the operating frequency exceeds 1.3 kHz, the CNT solution offers better gravimetric and volumetric power density due to the AC effects in copper wires. Composite based on both CNTs and copper has been explored as well to reduce the conductor weight, resistivity, and the sensitivity to temperature increase. According to [146], a 1-m, 25 AWG composite conductor with an electrical conductivity of 16–20 MS/m at 150°C has been successfully fabricated.

Experiments in [147] also showed that the composite produced by the newly industrially scalable method has high current carrying ability, electrical conductivity, and higher tensile strength compared with copper. There is good reason to believe that with advancements in production techniques, these new conductors have the potential to revolutionize the electric machine industry.

Regarding soft magnetic materials, the ideal core materials for aeronautical machines should have high magnetization saturation flux density (B_s), high curie temperature, high permeability, low electrical conductivity, low mass density, and low coercivity (H_c). Additionally, the material must be ductile and mechanically strong enough to be easily cut and withstand high mechanical stress. Soft magnetic composite (SMC) has been used in many publications since due to their reasonably low eddy current loss, low manufacturing cost, and the feasibility of being shaped into complex geometries [148]. Amorphous materials have also been gaining growing attention mainly due to their low H_c and core losses. However, the magnetization B_s of both materials is too low for aeronautical applications compared to pure CoFe steel. According to [149,150], CoFe offers a core loss level comparable to that of the best SiFe. The B_s level of CoFe is significantly higher than that of SiFe, allowing for a reduction in the size of components such as tooth width and stator yoke thickness, compensating for the increased mass density. Furthermore, a greater reduction in B_s at high operating temperatures is observed in SiFe materials [151] which may result in reduced output power in aeronautical machines that already designed near the material's limits. Therefore, PM machines with CoFe can achieve higher volumetric power density, and comparably high gravimetric power density, and are less vulnerable to high temperatures, making them an optimal candidate for most aeronautical electric machines.

To fully exploit the potential of CoFe, much research has been devoted to improving B_s and reducing the core losses of CoFe laminations.

In [152], CoFe materials obtained through different annealing techniques were compared, and their micrographic structures were also inspected. The test results showed that a higher B_s was achieved with the sample annealed at 850 °C for 3 h compared to those treated at 760 °C for 2 h. The tested B-H curves in [153] show that B_s of 2.45 can be reached with 34.5~35.5% of cobalt in the alloy which has been the limit of this material [154]. Efforts therefore have been made to explore new materials with higher B_s. A sample of a new compound was tested in [155], demonstrating a high B_s of 2.47 T and a coercivity close to the highest level found in CoFe. It was pointed out that as the purity of the alloy increases, the B_s can reach 2.8 $\pm$ 0.15 T. Additionally, the mass density of this new alloy is 93% that of CoFe, which could result in an even greater reduction in the weight of machine cores in the future.

The coercivity of CoFe has already been reduced to proper annealing during which the impurities (eg, carbon) can be eliminated and the grain can grow. Accoding to tested data shown in Figure 16, a low H_c of 60 A/m has already been achieved in commercially available high-performance CoFe alloy 1j22. To further reduce the hysteresis loss, the stress caused by cutting and punching has to be relieved. Experiments in [149] showed that after-cutting second heat treatment can mitigate the impact of residual stress, leading to a significant reduction of hysteresis losses. For eddy current loss reduction, the effectiveness of adding elements such as vanadium and chromium to the CoFe alloy has already been widely tested and adopted [153]. As reported in [156], increasing the vanadium content from 2% to 5% raises the resistivity of the new alloy to 0.7–0.75 μΩ·m, which is 75% higher than that of most commercially available CoFe alloys. Reducing the lamination thickness is another effective method to reduce the eddy current losses within the lamination as indicated in Figure 17.

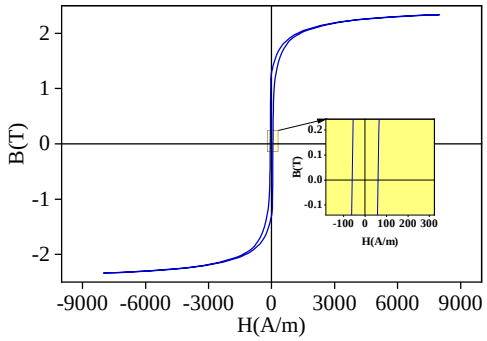

Figure 16. Tested hysteresis loop of high-performance CoFe alloy 1j22.

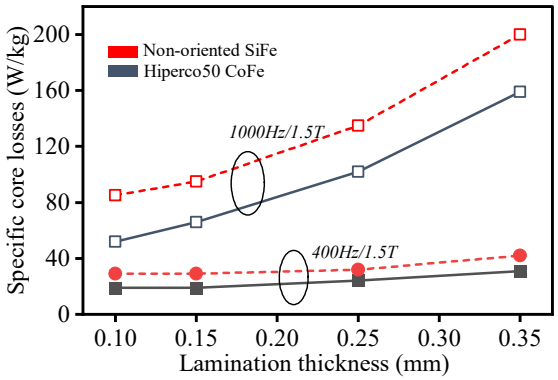

Figure 17. Core losses dependency on sheet thickness.

Recent publications show that pure iron steel sheets with a thickness of 4 µm have been obtained through continuous rolling processes [157]. Therefore, there is considerable potential for further reductions in alloy thickness, coupled with improvements in mechanical properties and manufacturing techniques. However, it is important to note that thinner lamination inevitably reduces the stacking factor (due to necessary inter-lamination gaps) and increases manufacturing difficulty due to the increased risk of deformation, both of which must be carefully considered during the design stage. To prevent the inter-lamination eddy current loss, an insulation layer between laminations is necessary. Two different coating and stacking processes have been investigated in [158] to search for optimal stacking methods. Varnish spraying before stacking has been proven to be a more effective method for achieving a reasonable stacking factor due to the more reliable and evenly distributed interlayer insulation. Furthermore, non-ideal factors the blur at the edges of the sheets and excessive pressure during stacking also give rise to the increase of interlaminar eddy current loss. New deblurring methods [159] and an electromechanical model for predicting interlaminar insulation quality are essential, particularly in high-speed machines.

4.1.2. Structural Materials

Structural components such as bearings, housing, shafts, and end caps can account for roughly half of the total weight [160]. The percentage can be even higher in some high-speed machines due to the lower torque requirements. Therefore, adopting lightweight structural materials has the potential to significantly improve the gravimetric power density of the machine without affecting the electromagnetic performance.

Conventionally, metal materials such as titanium alloys, aluminum (Al) alloys, stainless steel, and nickel alloys are widely used as structural materials in aeronautical electric machines due to their high strength-to-weight ratios, corrosion resistance, and generally high thermal conductivity [161]. However, replacing these metals with lighter materials such as magnesium alloys and composite materials remains an attractive option.

Magnesium (Mg) as the lightest engineered metal has a mass density close to the plastic and has been used to fabricate alloys for applications requiring weight reduction as early as the 1940s [162]. The concern about the risk of ignition has prohibited the adoption of Mg alloy. As more tests and research are carried out, the Mg alloy can certainly be used to replace Al to serve as the motor housing material for weight reduction [163].

In [164], carbon fiber composite combined with metal is used to build the hollow shaft instead of steel to reduce the weight as shown in Figure 18. Optimal processing and assembling techniques have been studied in detail making them suitable for massive production. A lightweight plastic motor housing is produced using the injection molding process [165], which can result in a 28% reduction in housing weight. Although the thermal conductivity is less than 1.6% of that of aluminum alloy, this drawback is mitigated by the innovative in-slot cooling design.

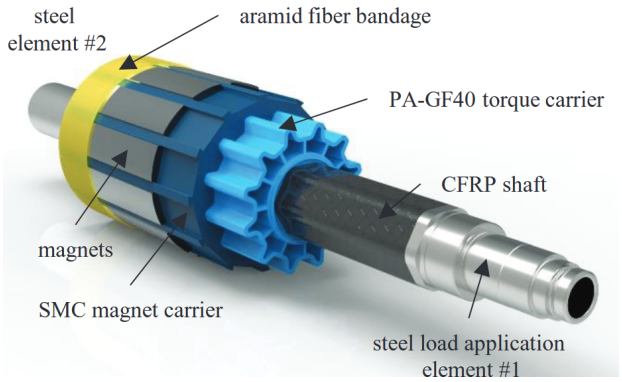

Figure 18. Lightweight PM rotor made of composites [164].

Although these lightweight materials can contribute to high power density, a multidisciplinary evaluation is necessary to ensure mechanical safety and sufficient thermal management capability due to their generally reduced mechanical strength and thermal conductivity.

4.1.3. Insulation Materials

Due to the increasing voltage levels and operating frequency of high power density aeronautic electric machines, more reliable insulation materials with limited thickness, enhanced thermal conductivity and temperature resistance capability are in greater demand than ever before. These improvements can not only increase the effective slot fill factor, reducing the risk of insulation failure caused by overheating but also simplify the cooling design, resulting in higher power density in the electric machine.

Most conventional polymer-based insulation materials consist of organic components such as polyimide, rubber, and plastic and cannot work at temperatures that are higher than 300 °C due to oxidation and decomposition issues. For high-temperature applications (eg, engine-integrated SGs), pure inorganic materials are considered a promising insulation option for high-power density PM machines as well due to their high thermal conductivity and high-temperature stability. For instance, ceramic materials are used as bearing coatings or rolling elements to effectively prevent electrical erosion caused by high stray currents [166]. A nickel layer is used to isolate the porous ceramic layer from the copper where the ceramic layer serves as the mechanical separator in [167]. The copper coils are then protected from oxidation under high temperatures.

Although these inorganic insulation offers much lower dielectric strength compared with conventional organic polymers [168], they can work for a long time under 500 °C. Another disadvantage of these materials is that they are too brittle to be formed into complex shapes making them unsuitable for wire insulations. To improve the overall performance of insulators, temperature-resistant inorganic insulating materials such as ceramic materials and mica can be used together with conventional organic insulators. These composites combine the benefits of both organic and inorganic insulators, offering high strength

and thermal conductivity, high breakdown voltage, resistance to high temperatures and corrosion, as well as moderate elasticity [169]. These features make them appealing for insulation in aeronautic electric machines.

A multilayer multifunctional insulation structure is proposed and optimized in [170]. It is confirmed that the multifunctional multi-layer structure can offer at least a 70% improvement in dielectric breakdown voltage compared to pure polyamide when insulation is thicker than 0.15 mm allowing for a reduction of insulation thickness. Functions such as electromagnetic interference shielding, heat dissipation, and corona barrier can be achieved by incorporating a specific layer as well. However, the thickness of this new insulator reported is higher than 0.15 mm making it difficult to use as an insulator of windings, it can be used to protect bus bars and transmission cables to reduce the overall weight.

It is reported in [171] that the thermal stability of an inorganic-organic nano-hybrid insulator can be significantly enhanced by ceramic fillers. Wires coated by this new nanocomposite can be easily bent and can withstand 1100 V alternating voltage after proper heat treatment. In [172], polymers filled with particles of various ceramic materials are compared. Tests proved that the thermal conductivity of the insulation composite has improved to 4~20 times that of pure polymer material. According to the thermal simulation results, the maximum winding temperature can be reduced by 21.7 °C, allowing for a further 10% increase in electric loading. It is verified in [173] that AlN and polymer composites offer over 10 times the thermal conductivity and 1.6 times the dielectric strength compared to conventional pure organic polymers. At least 50% power density improvement is predicted when adopting the new composite to insulate copper wire and magnetic steel. The aramid fiber is integrated with mica nanosheet to improve the electric and mechanical strength [174] offering higher tensile strength, breakdown strength, and improved high-temperature resistance compared with common pure arminid slot liner material [175].

With more experiments conducted and preparation techniques becoming more refined, thinner insulators with enhanced thermal and electrical performance will play a key role in future high-power density aeronautic machines.

4.2. Addictive Manufacturing Techniques

Additive manufacturing (AM) has been receiving rapidly growing attention from machine designers over the past decade, despite its high costs. The ability to create complex geometries that are unattainable with conventional machining methods makes AM a powerful solution for weight reduction and thermal performance enhancement of aeronautic machines.

Metal AM has already been used during the optimization of structural parts in electric machines to reduce the mass, and cost and improve the heat dissipation ability. In-slot lattice-structured aluminum alloy heat guides are employed to cool the active windings. The weight and introduced loss of these heat guides can effectively be reduced by AM technique [176]. Engineers from Diabatix designed a new water jacket for electric machines using artificial intelligence. The complex water jacket pattern realized through AM, can reduce the motor temperature by 21% while maintaining a lower pressure drop compared to conventional spiral designs. Different heat sink configurations are realized by AM in [177]. Configuration (d) shown in Figure 19, which cannot be fabricated by conventional methods, offers a relatively large heat transfer surface and an acceptable pressure drop, according to the comparison. The test results provide valuable insights into the design of cooling channels in liquid-cooled electric machines.

Apart from stationary components, AM can also be used to fabricate rotating parts. In [178], the rotor shaft with cavities and lattice is made by AM to reduce the rotor weight while maintaining the mechanical strength. Advanced topology optimization methods can be used to optimally distribute materials for designing other components, such as hollow shafts and rotor hubs [179], as demonstrated in [180].

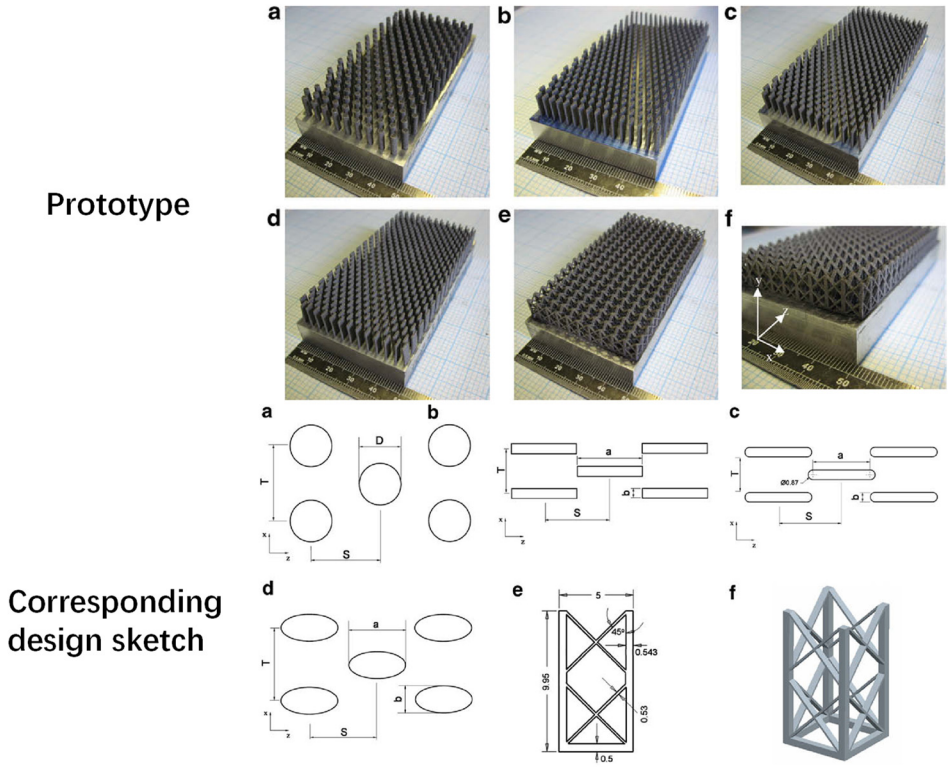

Figure 19. Different heat sink designs realized by AM [177].

In addition to the structural components, AM can also be used to construct the PMs, magnetic cores, and windings.

In [181], NdFeB magnetic particles are bonded with a eutectic alloy to improve the coercivity of heavy rare-earth-free magnets. Experiments show that the coercivity and its temperature coefficient are comparable to conventional sintered with rare earth materials. However, these bonded permanent magnets typically have lower working temperatures and offer lower remanence due to the introduction of the bonding materials. Furthermore, adopting PMs with complex shapes in aeronautic applications can lead to rotor mechanical instability, particularly under high-speed and high-temperature conditions.

As for magnetic cores, AM combined with SMC powders brings the potential of making complex shapes at a low cost. However, the solid structure can give rise to eddy current compared with conventional laminated configuration [182]. As mentioned earlier, the low B_s and permeability also make it even less appealing. High-performance CoFeV powder is used in [183] to study the potential of magnetic cores made by AM. Experiments show that compared with the inductor with a laminated core, the one with an addictive manufactured core has much higher core losses and lower inductance. It can be concluded that adopting AM to form magnetic cores based on powders will inevitably compromise the power density of electric machines. Therefore, other advantages such as weight reduction, utilization of space with irregular profiles, and improved thermal performance should outweigh the disadvantages if the AM cores are to be used in aeronautic electric machines. One good example can be found in [184] where structural-magnetic optimization is carried out based on the topology optimization method to reduce the weight of the rotor core of a high-speed PM machine. An optimized rotor core with 50% weight reduction while meeting the mechanical and electromagnetic requirements can be obtained. The cavities on the rotor back iron might be used as the flow channel of cooling air to reduce the temperature of magnets.

Finally, the motivations for using AM to form windings are mainly to increase the effective slot fill factor and the overall current density. To address the AC effects in multi-layer AM-fabricated flat conductors have been developed to minimize the leakage flux

linkage coupled to each layer. The shaped windings have demonstrated reduced AC copper losses and temperature while achieving higher current density. Additionally, AM enables smooth transposition in the end winding region of the coils which are located at different depths within the slots, helping to balance the inductance of various parallel branches. In [185], hollow conductors with two different alloys are made by multi-material AM. Low conductivity material is used for lower parts coils (near slot opening) with the upper part coils consisting of another alloy. Compared with uni-material coils, the hybrid conductor offers superior efficiency due to reduced AC copper losses. Such multi-material AM technique is adopted in [186] to effectively form the ceramic-coated conductors. Although the equivalent resistance of the AM winding is increased compared with stranded windings due to the porosity nature and limited manufacturing precision, the increased inter-coil thermal conductivity leads to over 50% winding temperature reduction.

Despite their enormous potential and benefits, metal AM and multi-material AM still face challenges such as dimensional precision, complex processing environments, and degraded electrical and mechanical performance, making it difficult to meet the requirements for producing active parts in high-performance aeronautic electric machines. Research and technological advancements are needed to address these challenges, enabling the production of fully additively manufactured electric machines with complex topologies, integrated cooling channels, and extremely lightweight designs.

4.3. Thermal Management

Proper cooling design is closely dependent on the machine working duty, loss distribution, accessibility to effective cooling agents, and the weight of the overall weight of the electrical system in aeronautic applications.

Forced air cooling is one of the simplest cooling configurations available. Compared with a liquid cooling system, several benefits can be obtained in air cooled system:

1. Additional weight introduced by the liquid channels (usually made of metal), pumps, and heat exchangers are eliminated.
2. The risk of liquid leakage is eliminated and the cooling system is simplified therefore maintenance costs can be reduced.
3. The possibility of cooling the rotor surface without significantly increasing the air friction losses since they are proportional to the mass density of the fluid.

The high-velocity, low-temperature air during flight can provide highly efficient cooling [187] for electric machines used in high-speed compressors, propulsion, and other applications where air is easily accessible. As shown in Figure 20 optimized fins can be attached to the stator housing to increase the convection surface area. As mentioned earlier, AM and topology optimization can be used to reduce the pressure drop, and the weight of the fins and to increase the convective heat transfer coefficients simultaneously. To get rid of the negative impact of thermal resistance between the stator core and housing, these cooling fins can be directly integrated with the stator core as demonstrated in Figure 20. The impact of these modifications of the stator core on the electromagnetic performance should be kept at a minimum.

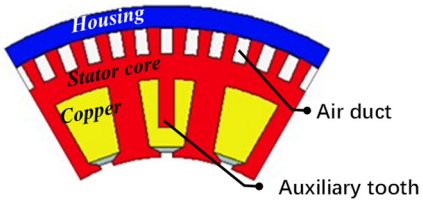

Figure 20. Cooling fins integrated with the stator core.

Despite the advantages of air cooling, more powerful cooling methods, such as single-phase liquid cooling and phase change cooling, are necessary in cases where the machine's loss density and operating temperature are extremely high.

Compared to the conventional stator liquid jacket cooling method, directly attaching the windings to heat conductors and cooling agents can be more effective in improving the power density of PM machines. In this case, highly compact flat wires are preferred over random stranded wires to reduce thermal resistance between conductors and prevent local thermal failures. The temperature in the end windings is typically higher than in the in-slot windings due to the increased thermal resistance between the end windings and the cooling agents. Therefore, measures such as shaft spray cooling, impingement cooling, and winding potting have been developed specifically to cool the end winding region. It is verified in [188] that the inserting of liquid cooling pipes among the end windings leads to a 25% temperature reduction in the region. These copper or oil cooling pipes can be integrated directly into the slots to extract heat from in-slot windings as well. This is especially suitable for machines with concentrated windings where there is no risk of interference between the cooling channels and end windings. It should be noted that these in-slot cooling channels and pipes will lead to potentially increased eddy current loss and reduced effective slot area. Therefore, thermal-electromagnetic analysis should be conducted to obtain an optimal solution. Another key to improving the thermal performance of the stator assembly is the impregnation quality. Therefore new insulation material with higher thermal conductivity and heat capacity should be explored not only to reduce the heat resistance in the slot but also to reduce the temperature impact. The increase of in-slot heat capacitance is especially important for machines with short operating duty cycles (e.g., electric-driven actuators) [189] or frequent overload operation (e.g., SGs in starting mode).

Considering the safety of PMs, additional thermal management on the rotor side becomes necessary to prevent the PMs from demagnetization since their temperature is very sensitive to rotor losses if only stator cooling is available [190]. The hollow shaft can be integrated with the rotor to provide additional heat extraction ability as shown in Figure 21. Inserting spider-shaped cooling pipes into the rotor back iron or rotor hub further reduces the thermal resistance between the magnets and coolant. Utilizing the hollow shaft structure, injection holes on the shaft in this case can be adapted to spray the liquid coolant on the end windings during rotation. In [191], rotating cooling channels and injection holes are connected in series. The existence of these cooling pipes allows for axial heat transferring which is difficult to achieve in laminated cores. However, external or integrated pumps (driven by the motor shaft) are always required in such liquid cooling systems to provide sufficient pressure for the coolant flow. This not only complicates the system but also results in additional losses. Another disadvantage is the increased risk of liquid leakage due to the degradation and corrosion of seals. Finally, the available coolant for the liquid cooling system includes aviation fuel and lubrication oil in the accessory gearbox. However, both fuel and lubrication oil degrade at high temperatures, increasing the risk of fouling on the surfaces of cooling channels and nozzles [192,193]. This not only limits the heat dissipation capacity of the oil cooling system but also poses the risk of channel blockages. Therefore, proper surface coatings, filtration, and the introduction of additives into the oil are necessary for effective oil cooling systems.

Furthermore, coolant that can vaporize and condense within a reasonably small temperature range can be sealed in a closed loop to transport heat effectively between the heat source and the heat sink. The liquid coolant indirectly absorbs the heat from the hotspot in the machine and vaporizes in the evaporator region as shown in Figure 22. The vapor then flows to the condenser where it can be liquified after being cooled either by air or oil. It is reported that very high equivalent thermal conductivity (5000 W/m·K to 100,000 W/m·K) can be achieved [194] with this heat pipe technology.

Since the ultimate cooling sources for aeronautic electric machines are still air and oil, which offer limited cooling capacity, it is not likely to reduce the temperature of electric machines globally. Besides, the metal containers with high mechanical and thermal performance also bring additional mass. Therefore it is only reasonable to adopt limited heat pipes in hotspots such as end windings, slot windings, and PMs to achieve a more

even temperature distribution within each component as was demonstrated in [195,196]. New emerging container materials and AM techniques can be used to design a heat pipe with both lightweight, customized shapes and satisfying heat transportation ability.

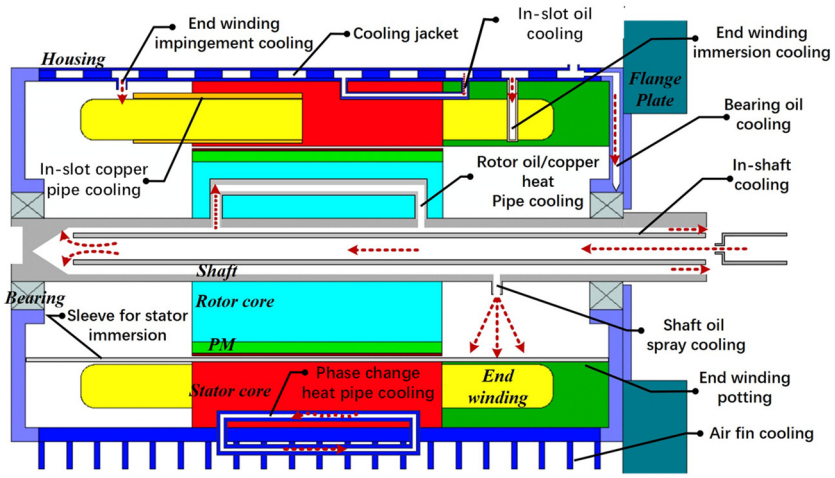

Figure 21. Typical cooling techniques for high-power density electric machines.

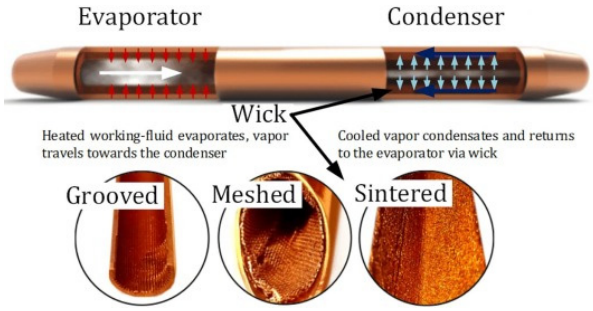

Figure 22. Schematic representation of Copper-Water heat pipe together with alternative wick constructions [194].

Comprehensive characterization and evaluation of losses in electric machines form the foundation for targeted thermal design. Following this, a thermal design incorporating multiple techniques can be implemented to avoid local hotspots and minimize the overall weight of the electric machine system. Furthermore, although it has been demonstrated in applications such as automobiles and home appliances that cooling systems can be made more compact and light [197], this may not be the case in aeronautic applications. When the electric drive system is used in extremely critical applications, such as propulsion, decoupling the cooling systems of the drive unit and the electric machines can prevent mutual electromagnetic interference and ensure that both modules operate within their temperature limitations.

5. Summary

This paper highlighted the vital role and the potential of the PMSMs in the ongoing shift towards electrified aircraft systems. Their ability to deliver high performance under stringent weight, volume, and environmental constraints makes them attractive in modern aviation. As research and technology continue to progress, PMSMs are expected to achieve higher efficiency, improved fault tolerance, and reduced environmental impact. Advancements in materials, cooling technologies, and optimization methods are critical for the successful implementation of all-electric and more-electric aircraft, pushing the boundaries of power density and operational efficiency in aeronautic applications.

Author Contributions: Investigation and analysis of the state-of-the-art works of literature: N.B. and C.L.; Development of the idea: N.B.; Draft of the manuscript: C.L.; Revision and proofreading: N.B., C.L. and Z.Z. All authors have read and agreed to the published version of the manuscript.

Funding: This research received no external funding.

Conflicts of Interest: The authors declare no conflict of interest.

Acronyms

AEA	All-Electric Aircraft
AM	Additive Manufacturing
APU	Auxiliary Power Unit
back-EMF	Back Electromotive Force
BLI	boundary layer ingestion
CNT	Carbon Nanotube
EHA	Electro-hydraulic Actuator
EMA	Electro-mechanical Actuator
FSCW	Fractional Slot Concentrated Winding
HEFS	Hybrid-excited Flux Switching
IDG	Integrated Drive Generator
IPM	Interior Permanent Magnet
LH_2	Liquid Hydrogen
ME	Main Exciter
MEA	More Electric Aircraft
OR	Outer Rotor
PEMFC	Polymer Electrolyte Membrane Fuel Cells
PM	Permanent Magnet
PMG	Permanent Magnet Generator
PMSM	Permanent Magnet Synchronous Machine
PMSG	PM Starter Generator
SIPM	Surface-inset Permanent Magnet
SMC	Soft Magnetic Composite
SOA	State-of-the-art
SPM	Surface-mounted Permanent Magnet
SG	Starter Generator

References

1. Weimer, J. Past, Present and Future of Aircraft Electrical Power Systems. In Proceedings of the 39th Aerospace Sciences Meeting and Exhibit, Reno, NV, USA, 8–11 January 2001; American Institute of Aeronautics and Astronautics: Reno, NV, USA, 2001.
2. Weimer, J.A. Electrical Power Technology for the More Electric Aircraft. In Proceedings of the AIAA/IEEE Digital Avionics Systems Conference, Fort Worth, TX, USA, 25–28 October 1993; pp. 445–450.
3. Spencer, K.M.; Martin, C.A. *More Electric Aircraft*; Investigation of Potential Fuel Cell Use in Aircraft; Institute for Defense Analyses: Alexandria, VA, USA, 2013; pp. 8–10.
4. Felder, J.L. NASA Electric Propulsion System Studies. 2015. Available online: https://ntrs.nasa.gov/citations/20160009274 (accessed on 23 July 2024).
5. Penner, J.E.; Lister, D.; Griggs, D.J.; Dokken, D.J.; McFarland, M. *Aviation and the Global Atmosphere: A Special Report of the Intergovernmental Panel on Climate Change*; Cambridge University Press: Cambridge, UK, 1999.
6. Hepperle, M. Electric Flight—Potential and Limitations. In Proceedings of the Energy Efficient Technologies and Concepts of Operation, Lisbon, Portugal, 22–24 October 2012.
7. Rohacs, J.; Rohacs, D. Energy Coefficients for Comparison of Aircraft Supported by Different Propulsion Systems. *Energy* **2020**, *191*, 116391. [CrossRef]
8. Bolam, R.C.; Vagapov, Y.; Anuchin, A. A Review of Electrical Motor Topologies for Aircraft Propulsion. In Proceedings of the 2020 55th International Universities Power Engineering Conference (UPEC), Turin, Italy, 1–4 September 2020; IEEE: Torino, Italy, 2020; pp. 1–6.
9. Misra, D.A. Technical Challenges and Barriers Affecting Turbo-Electric and Hybrid Electric Aircraft Propulsion. Available online: https://ntrs.nasa.gov/api/citations/20180004252/downloads/20180004252.pdf (accessed on 28 July 2024).

10. Committee on Propulsion and Energy Systems to Reduce Commercial Aviation Carbon Emissions; Aeronautics and Space Engineering Board; Division on Engineering and Physical Sciences; National Academies of Sciences, Engineering, and Medicine. *Commercial Aircraft Propulsion and Energy Systems Research: Reducing Global Carbon Emissions*; National Academies Press: Washington, DC, USA, 2016; p. 23490, ISBN 978-0-309-44096-7.
11. Welstead, J.; Felder, J.; Guynn, M.; Haller, B.; Tong, M.; Jones, S.; Ordaz, I.; Quinlan, J.; Mason, B. Overview of the NASA STARC-ABL (Rev. B) Advanced Concept. 2017. Available online: https://ntrs.nasa.gov/citations/20170005612 (accessed on 28 July 2024).
12. Spakovszky, Z.S.; Chen, Y.; Greitzer, E.M.; Cordero, Z.C.; Lang, J.H.; Kirtley, J.L.; Perreault, D.J.; Andersen, H.N.; Qasim, M.M.; Cuadrado, D.G.; et al. A Megawatt-Class Electrical Machine Technology Demonstrator For Turbo-Electric Propulsion. In Proceedings of the AIAA AVIATION 2023 Forum, San Diego, CA, USA, 12–16 June 2023.
13. Gao, Y.; Jausseme, C.; Huang, Z.; Yang, T. Hydrogen-Powered Aircraft: Hydrogen–Electric Hybrid Propulsion for Aviation. *IEEE Electrif. Mag.* **2022**, *10*, 17–26. [CrossRef]
14. Brand, J.; Sampath, S.; Shum, F.; Bayt, R.; Cohen, J. Potential Use of Hydrogen In Air Propulsion. In Proceedings of the AIAA International Air and Space Symposium and Exposition: The Next 100 Years, Reston, VA, USA, 14 July 2003; American Institute of Aeronautics and Astronautics: Orlando, FL, USA, 2003.
15. Sosounov, V.; Orlov, V. Experimental Turbofan Using Liquid Hydrogen and Liquid Natural Gas as Fuel. In Proceedings of the 26th Joint Propulsion Conference, Orlando, FL, USA, 16–18 July 1990; American Institute of Aeronautics and Astronautics: Orlando, FL, USA, 1990.
16. Brewer, G.D. LH2 Airport Requirements Study. 1976. Available online: https://ntrs.nasa.gov/api/citations/19770003090/downloads/19770003090.pdf (accessed on 28 July 2024).
17. O'Hayre, R.P.; Cha, S.-W.; Colella, W.G.; Prinz, F.B. *Fuel Cell Fundamentals*, 3rd ed.; John Wiley & Sons Inc.: Hoboken, NY, USA, 2016; ISBN 978-1-119-11415-4.
18. Adler, E.J.; Martins, J.R.R.A. Hydrogen-Powered Aircraft: Fundamental Concepts, Key Technologies, and Environmental Impacts. *Prog. Aerosp. Sci.* **2023**, *141*, 100922. [CrossRef]
19. Saufi Sulaiman, M.; Singh, B.; Mohamed, W.A.N.W. Experimental and Theoretical Study of Thermoelectric Generator Waste Heat Recovery Model for an Ultra-Low Temperature PEM Fuel Cell Powered Vehicle. *Energy* **2019**, *179*, 628–646. [CrossRef]
20. Finken, T.; Felden, M.; Hameyer, K. Comparison and Design of Different Electrical Machine Types Regarding Their Applicability in Hybrid Electrical Vehicles. In Proceedings of the 2008 18th International Conference on Electrical Machines, Vilamoura, Portugal, 6–9 September 2008; pp. 1–5.
21. Podmiljšak, B.; Saje, B.; Jenuš, P.; Tomše, T.; Kobe, S.; Žužek, K.; Šturm, S. The Future of Permanent-Magnet-Based Electric Motors: How Will Rare Earths Affect Electrification? *Materials* **2024**, *17*, 848. [CrossRef]
22. Gieras, J.F. *Permanent Magnet Motor Technology: Design and Applications*, 3rd ed.; CRC Press: Boca Raton, FL, USA, 2009; ISBN 978-0-429-29273-6.
23. Ford, A.W. Brushless Generators for Aircraft—A Review of Current Developments. *Proc. IEE-Part Power Eng.* **1962**, *109*, 437–452. [CrossRef]
24. Pardo-Vicente, M.A.; Guerrero, J.M.; Platero, C.A.; Sánchez-Férnandez, J.A. Contactless Rotor Ground Fault Detection Method for Brushless Synchronous Machines Based on an AC/DC Rotating Current Sensor. *Sensors* **2023**, *23*, 9065. [CrossRef]
25. Jahns, T.M.; Soong, W.L. Pulsating Torque Minimization Techniques for Permanent Magnet AC Motor Drives—A Review. *IEEE Trans. Ind. Electron.* **1996**, *43*, 321–330. [CrossRef]
26. Mun, J.-M.; Park, G.-J.; Seo, S.; Kim, D.-W.; Kim, Y.-J.; Jung, S.-Y. Design Characteristics of IPMSM With Wide Constant Power Speed Range for EV Traction. *IEEE Trans. Magn.* **2017**, *53*, 1–4. [CrossRef]
27. Huynh, T.A.; Hsieh, M.-F. Comparative Study of PM-Assisted SynRM and IPMSM on Constant Power Speed Range for EV Applications. *IEEE Trans. Magn.* **2017**, *53*, 1–6. [CrossRef]
28. Sarlioglu, B.; Morris, C.T.; Han, D.; Li, S. Benchmarking of Electric and Hybrid Vehicle Electric Machines, Power Electronics, and Batteries. In Proceedings of the 2015 International Aegean Conference on Electrical Machines & Power Electronics (ACEMP), 2015 International Conference on Optimization of Electrical & Electronic Equipment (OPTIM) & 2015 International Symposium on Advanced Electromechanical Motion Systems (ELECTROMOTION), Side, Turkey, 2–4 September 2015; pp. 519–526.
29. Gerada, C.; Galea, M.; Kladas, A. Electrical Machines for Aerospace Applications. In Proceedings of the 2015 IEEE Workshop on Electrical Machines Design, Control and Diagnosis (WEMDCD), Turin, Italy, 26–27 March 2015; pp. 79–84.
30. Murakami, H.; Honda, Y.; Kiriyama, H.; Morimoto, S.; Takeda, Y. The Performance Comparison of SPMSM, IPMSM and SynRM in Use as Air-Conditioning Compressor. In Proceedings of the Conference Record of the 1999 IEEE Industry Applications Conference. Thirty-Forth IAS Annual Meeting (Cat. No. 99CH36370), Phoenix, AZ, USA, 3–7 October 1999; Volume 2, pp. 840–845.
31. Burress, T.A.; Coomer, C.L.; Campbell, S.L.; Seiber, L.E.; Marlino, L.D.; Staunton, R.H.; Cunningham, J.P. *Evaluation of the 2007 Toyota Camry Hybrid Synergy Drive System*; Oak Ridge National Lab. (ORNL): Oak Ridge, TN, USA, 2008; p. 928684.
32. Ayers, C.W. *Evaluation of 2004 Toyota Prius Hybrid Electric Drive System Interim Report*; Oak Ridge National Lab. (ORNL): Oak Ridge, TN, USA, 2004; p. 885776.
33. Burress, T.A.; Campbell, S.L.; Coomer, C.; Ayers, C.W.; Wereszczak, A.A.; Cunningham, J.P.; Marlino, L.D.; Seiber, L.E.; Lin, H.-T. *Evaluation of the 2010 Toyota Prius Hybrid Synergy Drive System*; Oak Ridge National Lab. (ORNL): Oak Ridge, TN, USA, 2011; p. 1007833.

34. Goli, C.S.; Manjrekar, M.; Essakiappan, S.; Sahu, P.; Shah, N. Landscaping and Review of Traction Motors for Electric Vehicle Applications. In Proceedings of the 2021 IEEE Transportation Electrification Conference & Expo (ITEC), Chicago, IL, USA, 21–25 June 2021; pp. 162–168.
35. Hsu, J.S. *Report on Toyota/Prius Motor Torque-Capability, Torque-Property, No-Load Back EMF, and Mechanical Losses*; Oak Ridge National Lab. (ORNL): Oak Ridge, TN, USA, 2004; p. 885669.
36. Burress, T. Electrical Performance, Reliability Analysis, and Characterization. Available online: https://www.energy.gov/sites/prod/files/2017/06/f34/edt087_burress_2017_o.pdf (accessed on 1 September 2024).
37. Burress, T. Benchmarking EV and HEV Technologies. Available online: https://energy.gov/sites/prod/files/2014/07/f17/ape006_burress_2014_p.pdf (accessed on 1 September 2024).
38. Gierczynski, M.; Grzesiak, L.M. Comparative Analysis of the Steady-State Model Including Non-Linear Flux Linkage Surfaces and the Simplified Linearized Model When Applied to a Highly-Saturated Permanent Magnet Synchronous Machine—Evaluation Based on the Example of the BMW I3 Traction Motor. *Energies* **2021**, *14*, 2343. [CrossRef]
39. Quoc, V.D.; Minh, D.B. Analysis of Power and Torque for the IPM Motors with High Flux Density in Stator. *Adv. Electr. Electron. Eng.* **2023**, *21*, 59.
40. Zheng, S.; Zhu, X.; Xiang, Z.; Xu, L.; Zhang, L.; Lee, C.H.T. Technology Trends, Challenges, and Opportunities of Reduced-Rare-Earth PM Motor for Modern Electric Vehicles. *Green Energy Intell. Transp.* **2022**, *1*, 100012. [CrossRef]
41. Ocak, O.; Gulec, M.; Aydin, M. Performance Comparison of Different IPM Motor Topologies for Spindle Motor Drives. In Proceedings of the IECON 2021—47th Annual Conference of the IEEE Industrial Electronics Society, Toronto, ON, Canada, 13–16 October 2021; pp. 1–6.
42. Swanke, J.; Bobba, D.; Jahns, T.M.; Sarlioglu, B. Comparison of Modular PM Propulsion Machines for High Power Density. In Proceedings of the 2019 IEEE Transportation Electrification Conference and Expo (ITEC), Detroit, MI, USA, 19–21 June 2019; pp. 1–7.
43. Jordan, S.; Baker, N.J. Air-Cooled, High Torque Machines for Aerospace Applications. In Proceedings of the 8th IET International Conference on Power Electronics, Machines and Drives (PEMD 2016), Glasgow, UK, 19–21 April 2016; pp. 1–6.
44. Ito, M.; Suto, T.; Takahashi, A.; Hara, T.; Iwano, R. Development of a High Power Density In-Wheel Motor Using Halbach Array Magnets. In Proceedings of the 2022 International Conference on Electrical Machines (ICEM), Valencia, Spain, 5–8 September 2022; pp. 355–360.
45. Bianchini, C.; Immovilli, F.; Lorenzani, E.; Bellini, A.; Davoli, M. Review of Design Solutions for Internal Permanent-Magnet Machines Cogging Torque Reduction. *IEEE Trans. Magn.* **2012**, *48*, 2685–2693. [CrossRef]
46. Sitapati, K.; Krishnan, R. Performance Comparisons of Radial and Axial Field, Permanent-Magnet, Brushless Machines. *IEEE Trans. Ind. Appl.* **2001**, *37*, 1219–1226. [CrossRef]
47. Cavagnino, A.; Lazzari, M.; Profumo, F.; Tenconi, A. A Comparison between the Axial Flux and the Radial Flux Structures for PM Synchronous Motors. *IEEE Trans. Ind. Appl.* **2002**, *38*, 1517–1524. [CrossRef]
48. Zhang, B.; Seidler, T.; Dierken, R.; Doppelbauer, M. Development of a Yokeless and Segmented Armature Axial Flux Machine. *IEEE Trans. Ind. Electron.* **2016**, *63*, 2062–2071. [CrossRef]
49. Nishanth, F.; Van Verdeghem, J.; Severson, E.L. A Review of Axial Flux Permanent Magnet Machine Technology. *IEEE Trans. Ind. Appl.* **2023**, *59*, 3920–3933. [CrossRef]
50. Zhang, Z.; Yan, Y.; Yang, S.; Bo, Z. Principle of Operation and Feature Investigation of a New Topology of Hybrid Excitation Synchronous Machine. *IEEE Trans. Magn.* **2008**, *44*, 2174–2180. [CrossRef]
51. Chen, Z.; Wang, B.; Chen, Z.; Yan, Y. Comparison of Flux Regulation Ability of the Hybrid Excitation Doubly Salient Machines. *IEEE Trans. Ind. Electron.* **2014**, *61*, 3155–3166. [CrossRef]
52. Geng, W.; Zhang, Z.; Jiang, K.; Yan, Y. A New Parallel Hybrid Excitation Machine: Permanent-Magnet/Variable-Reluctance Machine With Bidirectional Field-Regulating Capability. *IEEE Trans. Ind. Electron.* **2015**, *62*, 1372–1381. [CrossRef]
53. Nasr, A.; Hlioui, S.; Gabsi, M.; Mairie, M.; Lalevee, D. Design Optimization of a Hybrid-Excited Flux-Switching Machine for Aircraft-Safe DC Power Generation Using a Diode Bridge Rectifier. *IEEE Trans. Ind. Electron.* **2017**, *64*, 9896–9904. [CrossRef]
54. Hua, W.; Cheng, M.; Zhang, G. A Novel Hybrid Excitation Flux-Switching Motor for Hybrid Vehicles. *IEEE Trans. Magn.* **2009**, *45*, 4728–4731. [CrossRef]
55. Xiong, L.; Ge, H.; Zhou, B.; Wang, K.; Jiang, S.; Zhou, X.; Shi, H. Torque Ripple Reduction Strategy for Doubly Salient Electromagnetic Machine Based on Current Given Function. *IEEE J. Emerg. Sel. Top. Power Electron.* **2022**, *10*, 7486–7501. [CrossRef]
56. Mazzoleni, M.; Di Rito, G.; Previdi, F. *Electro-Mechanical Actuators for the More Electric Aircraft*; Advances in Industrial Control; Springer International Publishing: Cham, Switzerland, 2021; ISBN 978-3-030-61798-1.
57. Qiao, G.; Liu, G.; Shi, Z.; Wang, Y.; Ma, S.; Lim, T.C. A Review of Electromechanical Actuators for More/All Electric Aircraft Systems. *Proc. Inst. Mech. Eng. Part C J. Mech. Eng. Sci.* **2018**, *232*, 4128–4151. [CrossRef]
58. Boglietti, A.; Cavagnino, A.; Tenconi, A.; Vaschetto, S.; di Torino, P. The Safety Critical Electric Machines and Drives in the More Electric Aircraft: A Survey. In Proceedings of the 2009 35th Annual Conference of IEEE Industrial Electronics, Porto, Portugal, 3–5 November 2009; pp. 2587–2594.
59. Maré, J.-C.; Fu, J. Review on Signal-by-Wire and Power-by-Wire Actuation for More Electric Aircraft. *Chin. J. Aeronaut.* **2017**, *30*, 857–870. [CrossRef]

60. Huang, L.; Yu, T.; Jiao, Z.; Li, Y. Active Load-Sensitive Electro-Hydrostatic Actuator for More Electric Aircraft. *Appl. Sci.* **2020**, *10*, 6978. [CrossRef]
61. Garcia, A.; Cusido, I.; Rosero, J.A.; Ortega, J.A.; Romeral, L. Reliable Electro-Mechanical Actuators in Aircraft. *IEEE Aerosp. Electron. Syst. Mag.* **2008**, *23*, 19–25. [CrossRef]
62. Atallah, K.; Caparrelli, F.; Bingham, C.M.; Schofield, N.; Howe, D.; Mellor, P.H.; Maxwell, C.; Moorhouse, D.; Whitley, C. Permanent Magnet Brushless Drives for Aircraft Flight Control Surface Actuation. In Proceedings of the IEE Colloquium on Electrical Machines and Systems for the More Electric Aircraft (Ref. No. 1999/180), London, UK, 9 November 1999; pp. 8/1–8/5.
63. Maré, J.-C. Review and Analysis of the Reasons Delaying the Entry into Service of Power-by-Wire Actuators for High-Power Safety-Critical Applications. *Actuators* **2021**, *10*, 233. [CrossRef]
64. Bartlett, H.L.; Lawson, B.E.; Goldfarb, M. Optimal Transmission Ratio Selection for Electric Motor Driven Actuators With Known Output Torque and Motion Trajectories. *J. Dyn. Syst. Meas. Control* **2017**, *139*, 101013. [CrossRef]
65. Ismagilov, F.R.; Vavilov, V.E.; Sayakhov, I.F. High-Torque Motor for a Gearless Electromechanical Actuator. In Proceedings of the 2019 26th International Workshop on Electric Drives: Improvement in Efficiency of Electric Drives (IWED), Moscow, Russia, 30 January–2 February 2019; pp. 1–5.
66. Gerada, C.; Bradley, K.J. Integrated PM Machine Design for an Aircraft EMA. *IEEE Trans. Ind. Electron.* **2008**, *55*, 3300–3306. [CrossRef]
67. Huang, X.; Gerada, C.; Goodman, A.; Bradley, K.; Zhang, H.; Fang, Y. A Brushless DC Motor Design for an Aircraft Electro-Hydraulic Actuation System. In Proceedings of the 2011 IEEE International Electric Machines & Drives Conference (IEMDC), Niagara Falls, ON, Canada, 15–18 May 2011; pp. 1153–1158.
68. Villani, M.; Tursini, M.; Fabri, G.; Castellini, L. High Reliability Permanent Magnet Brushless Motor Drive for Aircraft Application. *IEEE Trans. Ind. Electron.* **2012**, *59*, 2073–2081. [CrossRef]
69. Bianchi, N.; Bolognani, S. Fault -Tolerant PM Motors in Automotive Applications. In Proceedings of the 2005 IEEE Vehicle Power and Propulsion Conference, Chicago, IL, USA, 7–9 September 2005; pp. 747–755.
70. EL-Refaie, A.M. Fractional-Slot Concentrated-Windings Synchronous Permanent Magnet Machines: Opportunities and Challenges. *IEEE Trans. Ind. Electron.* **2010**, *57*, 107–121. [CrossRef]
71. Sarigiannidis, A.G.; Beniakar, M.E.; Kakosimos, P.E.; Kladas, A.G.; Papini, L.; Gerada, C. Fault Tolerant Design of Fractional Slot Winding Permanent Magnet Aerospace Actuator. *IEEE Trans. Transp. Electrif.* **2016**, *2*, 380–390. [CrossRef]
72. Ismagilov, F.R.; Vavilov, V.Y.; Karimov, R.D.; Ayguzina, V.V.; Kammermann, J.; Bolvashenkov, I.; Herzog, H.-G. Design of a Six-Phase Fault-Tolerant Electric Motor for an Aircraft Fuel Pump. In Proceedings of the 2019 Fourteenth International Conference on Ecological Vehicles and Renewable Energies (EVER), Monte-Carlo, Monaco, 8–10 May 2019; pp. 1–6.
73. Atkinson, G.J.; Mecrow, B.C.; Jack, A.G.; Atkinson, D.J.; Sangha, P.; Benarous, M. The Analysis of Losses in High-Power Fault-Tolerant Machines for Aerospace Applications. *IEEE Trans. Ind. Appl.* **2006**, *42*, 1162–1170. [CrossRef]
74. Jiang, X.; Huang, W.; Cao, R.; Hao, Z.; Jiang, W. Electric Drive System of Dual-Winding Fault-Tolerant Permanent-Magnet Motor for Aerospace Applications. *IEEE Trans. Ind. Electron.* **2015**, *62*, 7322–7330. [CrossRef]
75. Mecrow, B.C.; Jack, A.G.; Atkinson, D.J.; Green, S.R.; Atkinson, G.J.; King, A.; Green, B. Design and Testing of a Four-Phase Fault-Tolerant Permanent-Magnet Machine for an Engine Fuel Pump. *IEEE Trans. Energy Convers.* **2004**, *19*, 671–678. [CrossRef]
76. Huang, L.; Hao, S.; Li, D.; Wang, C.; Cheng, Y. Analysis and Design of a Flat Wire PM Machine with Module-Combined and Hollowed-out Stator for Aviation Electric Pump. In Proceedings of the 2023 26th International Conference on Electrical Machines and Systems (ICEMS), Zhuhai, China, 5–8 November 2023; pp. 3221–3226.
77. Zhang, F.; Du, G.; Wang, T.; Liu, G.; Cao, W. Rotor Retaining Sleeve Design for a 1.12-MW High-Speed PM Machine. *IEEE Trans. Ind. Appl.* **2015**, *51*, 3675–3685. [CrossRef]
78. Gao, P.; Gu, Y.; He, Y.; Gerada, D.; Wang, X.; Gerada, C. Mechanical Strength Analysis and Ptimization of Metallic Sleeve in High-Speed Permanent Magnet Synchronous Machines. *Int. J. Appl. Electromagn. Mech.* **2020**, *63*, 343–359. [CrossRef]
79. Binder, A.; Schneider, T.; Klohr, M. Fixation of Buried and Surface-Mounted Magnets in High-Speed Permanent-Magnet Synchronous Machines. *IEEE Trans. Ind. Appl.* **2006**, *42*, 1031–1037. [CrossRef]
80. Wang, W.; Li, Y.; Huan, D.; Chen, X.; Liu, H.; Li, Y.; Li, L. Research on Stress Design and Manufacture of the Fiber-Reinforced Composite Sleeve for the Rotor of High-Speed Permanent Magnet Motor. *Energies* **2022**, *15*, 2467. [CrossRef]
81. Xie, X.; Liao, C.; Zhang, Z. Design Considerations of High-Speed PMSM with Nonuniform Two-Segment Halbach Magnet Array. *IEEE Trans. Magn.* **2024**, *60*, 1–6. [CrossRef]
82. Tong, W.; Sun, R.; Zhang, C.; Wu, S.; Tang, R. Loss and Thermal Analysis of a High-Speed Surface-Mounted PMSM With Amorphous Metal Stator Core and Titanium Alloy Rotor Sleeve. *IEEE Trans. Magn.* **2019**, *55*, 8102104. [CrossRef]
83. Zhang, C.; Chen, L.; Yu, S.; Ma, X.; Wang, X.; Tang, R. Performance Characteristics of High Speed Permanent Magnet Machine with Different Rotor Retaining Sleeve. In Proceedings of the 2019 22nd International Conference on Electrical Machines and Systems (ICEMS), Harbin, China, 11–14 August 2019; pp. 1–5.
84. Li, W.; Qiu, H.; Zhang, X.; Cao, J.; Yi, R. Analyses on Electromagnetic and Temperature Fields of Superhigh-Speed Permanent-Magnet Generator with Different Sleeve Materials. *IEEE Trans. Ind. Electron.* **2014**, *61*, 3056–3063. [CrossRef]
85. Zhang, Z.; Deng, Z.; Sun, Q.; Peng, C.; Gu, Y.; Pang, G. Analytical Modeling and Experimental Validation of Rotor Harmonic Eddy-Current Loss in High-Speed Surface-Mounted Permanent Magnet Motors. *IEEE Trans. Magn.* **2019**, *55*, 1–11. [CrossRef]

86. Bianchi, N.; Fornasiero, E. Index of Rotor Losses in Three-Phase Fractional-Slot Permanent Magnet Machines. *IET Electr. Power Appl.* **2009**, *3*, 381–388. [CrossRef]
87. Zhou, F.; Shen, J.; Fei, W.; Lin, R. Study of Retaining Sleeve and Conductive Shield and Their Influence on Rotor Loss in High-Speed PM BLDC Motors. *IEEE Trans. Magn.* **2006**, *42*, 3398–3400. [CrossRef]
88. Wang, Y.; Ma, J.; Liu, C.; Lei, G.; Guo, Y.; Zhu, J. Reduction of Magnet Eddy Current Loss in PMSM by Using Partial Magnet Segment Method. *IEEE Trans. Magn.* **2019**, *55*, 8105105. [CrossRef]
89. Gerada, D.; Mebarki, A.; Brown, N.L.; Gerada, C.; Cavagnino, A.; Boglietti, A. High-Speed Electrical Machines: Technologies, Trends, and Developments. *IEEE Trans. Ind. Electron.* **2014**, *61*, 2946–2959. [CrossRef]
90. Wang, Y.; Zhu, Z.-Q.; Feng, J.; Guo, S.; Li, Y.; Wang, Y. Rotor Stress Analysis of High-Speed Permanent Magnet Machines With Segmented Magnets Retained by Carbon-Fibre Sleeve. *IEEE Trans. Energy Convers.* **2021**, *36*, 971–983. [CrossRef]
91. Hu, Y.; Zhu, S.; Xu, L.; Jiang, B. Reduction of Torque Ripple and Rotor Eddy Current Losses by Closed Slots Design in a High-Speed PMSM for EHA Applications. *IEEE Trans. Magn.* **2022**, *58*, 1–6. [CrossRef]
92. Huang, Z.; Fang, J. Multiphysics Design and Optimization of High-Speed Permanent-Magnet Electrical Machines for Air Blower Applications. *IEEE Trans. Ind. Electron.* **2016**, *63*, 2766–2774. [CrossRef]
93. Kluyskens, V.; Dehez, B.; Ahmed, H.B. Dynamical Electromechanical Model for Magnetic Bearings. *IEEE Trans. Magn.* **2007**, *43*, 3287–3292. [CrossRef]
94. Hong, D.-K.; Woo, B.-C.; Lee, J.-Y.; Koo, D.-H. Ultra High Speed Motor Supported by Air Foil Bearings for Air Blower Cooling Fuel Cells. *IEEE Trans. Magn.* **2012**, *48*, 871–874. [CrossRef]
95. Li, S.; Li, Y.; Choi, W.; Sarlioglu, B. High-Speed Electric Machines: Challenges and Design Considerations. *IEEE Trans. Transp. Electrif.* **2016**, *2*, 2–13. [CrossRef]
96. Du, G.; Zhou, Q.; Liu, S.; Huang, N.; Chen, X. Multiphysics Design and Multiobjective Optimization for High-Speed Permanent Magnet Machines. *IEEE Trans. Transp. Electrif.* **2020**, *6*, 1084–1092. [CrossRef]
97. Uzhegov, N.; Kurvinen, E.; Nerg, J.; Pyrhönen, J.; Sopanen, J.T.; Shirinskii, S. Multidisciplinary Design Process of a 6-Slot 2-Pole High-Speed Permanent-Magnet Synchronous Machine. *IEEE Trans. Ind. Electron.* **2016**, *63*, 784–795. [CrossRef]
98. Xie, B.; Zhang, Y.; Xu, Z.; Zhang, F. Rotor Multidisciplinary Optimization of High Speed PMSM Based on Multi-Fidelity Surrogate Model and Gradient Sequential Sampling. *IEEE Trans. Energy Convers.* **2023**, *38*, 859–868. [CrossRef]
99. Xu, Y.; Xu, Z.; Wang, H.; Liu, W. Research on Magnetic-Fluid-Thermal-Stress Multi-Field Bidirectional Coupling of High Speed Permanent Magnet Synchronous Motors. *Case Stud. Therm. Eng.* **2024**, *54*, 104012. [CrossRef]
100. Hong, D.-K.; Woo, B.-C.; Jeong, Y.-H.; Koo, D.-H.; Ahn, C.-W. Development of an Ultra High Speed Permanent Magnet Synchronous Motor. *Int. J. Precis. Eng. Manuf.* **2013**, *14*, 493–499. [CrossRef]
101. Jiao, N.; Liu, W.; Meng, T.; Peng, J.; Mao, S. Design and Control of a Two-Phase Brushless Exciter for Aircraft Wound-Rotor Synchronous Starter/Generator in the Starting Mode. *IEEE Trans. Power Electron.* **2016**, *31*, 4452–4461. [CrossRef]
102. Wang, Y.; Nuzzo, S.; Zhang, H.; Zhao, W.; Gerada, C.; Galea, M. Challenges and Opportunities for Wound Field Synchronous Generators in Future More Electric Aircraft. *IEEE Trans. Transp. Electrif.* **2020**, *6*, 1466–1477. [CrossRef]
103. Secunde, R. Integrated Engine-Generator for Aircraft Secondary Power. In Proceedings of the 8th Joint Propulsion Specialist Conference, New Orleans, LA, USA, 29 November–1 December 1972. [CrossRef]
104. Richter, E.; Neumann, T.W. Jet Engine Integrated Generator. *J. Energy* **1982**, *6*, 45–48. [CrossRef]
105. Royce, R. *The Jet Engine*; Rolls-Royce Plc: London, UK, 2005; ISBN 978-0-902121-23-2.
106. Franco, A.; McGarvey, J.; Kane, D.; Salata, M. Flux Shunt Wave Shape Control Arrangement for Permanent Magnet Machines. U.S. Patent No. 6,750,628, 15 June 2004.
107. el-Rafaie, A.M.F.; Kern, J.M.; Shah, M.R. Fault-Tolerant Permanent Magnet Machine with Reconfigurable Stator Core Slot Flux Paths. U.S. Patent No. 7,605,503, 20 October 2010.
108. Wang, B.; Liu, Y.; Vakil, G.; Yang, T.; Zhang, Z. Feasibility of Permanent Magnet Fault Tolerant Machines for Aircraft Starter/Generator Systems. In Proceedings of the 2020 International Conference on Electrical Machines (ICEM), Gothenburg, Sweden, 23–26 August 2020; Volume 1, pp. 2104–2110.
109. He, Y.; Zhao, W.; Tang, H.; Ji, J. Auxiliary Teeth Design to Reduce Short-Circuit Current in Permanent Magnet Generators. *CES Trans. Electr. Mach. Syst.* **2020**, *4*, 198–205. [CrossRef]
110. Papini, L.; Gerada, C.; Goodman, A. Analysis of a Closed-Slot PM Machine. In Proceedings of the 2013 International Electric Machines & Drives Conference, Chicago, IL, USA, 12–15 May 2013; pp. 578–585.
111. Wu, S.; Chen, Q.; Li, Q.; Liu, X.; Zhang, H.; Lin, L. Design of Aviation High Impedance Permanent Magnet Synchronous Generator. *Math. Probl. Eng.* **2021**, *2021*, 6667877. [CrossRef]
112. Jiang, Y.; Zhang, Z.; Jiang, W.; Geng, W.; Huang, J. Three-Phase Current Injection Method for Mitigating Turn-to-Turn Short-Circuit Fault in Concentrated-Winding Permanent Magnet Aircraft Starter Generator. *IET Electr. Power Appl.* **2018**, *12*, 566–574. [CrossRef]
113. Sun, L.; Zhang, Z.; Yu, L.; Gu, X.; Vansompel, H.; Sergeant, P. Design and Analysis of Hybrid Excitation Generators for Aircraft Applications Under Limiting Open-Circuit Voltage. *IEEE Trans. Transp. Electrif.* **2022**, *8*, 3390–3400. [CrossRef]
114. Zhu, Z.Q.; Pothi, N.; Xu, P.L.; Ren, Y. Uncontrolled Generator Fault Protection of Novel Hybrid-Excited Doubly Salient Synchronous Machines With Field Excitation Current Control. *IEEE Trans. Ind. Appl.* **2019**, *55*, 3598–3606. [CrossRef]

115. Hoang, E.; Lecrivain, M.; Gabsi, M. A New Structure of a Switching Flux Synchronous Polyphased Machine with Hybrid Excitation. In Proceedings of the 2007 European Conference on Power Electronics and Applications, Aalborg, Denmark, 2–5 September 2007; pp. 1–8.
116. Afinowi, I.A.A.; Zhu, Z.Q.; Guan, Y.; Mipo, J.C.; Farah, P. Hybrid-Excited Doubly Salient Synchronous Machine With Permanent Magnets Between Adjacent Salient Stator Poles. *IEEE Trans. Magn.* **2015**, *51*, 1–9. [CrossRef]
117. Pothi, N.; Zhu, Z.Q.; Afinowi, I.A.A.; Lee, B.; Ren, Y. Control Strategy for Hybrid-Excited Switched-Flux Permanent Magnet Machines. *IET Electr. Power Appl.* **2015**, *9*, 612–619. [CrossRef]
118. Wang, Q.; Niu, S.; Luo, X. A Novel Hybrid Dual-PM Machine Excited by AC With DC Bias for Electric Vehicle Propulsion. *IEEE Trans. Ind. Electron.* **2017**, *64*, 6908–6919. [CrossRef]
119. Li, J.; Zhang, Z.; Lu, J.; Liu, Y.; Chen, Z. Design and Characterization of a Single-Phase Main Exciter for Aircraft Wound-Rotor Synchronous Starter–Generator. *IEEE Trans. Magn.* **2018**, *54*, 1–5. [CrossRef]
120. Gu, X.; Zhang, Z.; Bianchi, N.; Jiang, W. Enhanced Power Multi Excitation Brushless DC Generator Using Parallel Magnetic Circuits. *IEEE Trans. Transp. Electrif.* **2024**, 1. [CrossRef]
121. Brown, G. Weights and Efficiencies of Electric Components of a Turboelectric Aircraft Propulsion System. In Proceedings of the 49th AIAA Aerospace Sciences Meeting including the New Horizons Forum and Aerospace Exposition, Orlando, FL, USA, 4–7 January 2011; American Institute of Aeronautics and Astronautics: Reno, NV, USA, 2011.
122. Golovanov, D.; Gerada, D.; Sala, G.; Degano, M.; Trentin, A.; Connor, P.H.; Xu, Z.; Rocca, A.L.; Galassini, A.; Tarisciotti, L.; et al. 4-MW Class High-Power-Density Generator for Future Hybrid-Electric Aircraft. *IEEE Trans. Transp. Electrif.* **2021**, *7*, 2952–2964. [CrossRef]
123. Yoon, A.; Arastu, F.; Lohan, D.; Xiao, J.; Haran, K. Direct-Drive Electric Motor for STARC-ABL Tail-Cone Propulsor. In Proceedings of the 2019 AIAA/IEEE Electric Aircraft Technologies Symposium (EATS), Indianapolis, IN, USA, 22–24 August 2019; pp. 1–10.
124. Zhang, X.; Bowman, C.L.; O'Connell, T.C.; Haran, K.S. Large Electric Machines for Aircraft Electric Propulsion. *IET Electr. Power Appl.* **2018**, *12*, 767–779. [CrossRef]
125. Yoon, A.; Yi, X.; Martin, J.; Chen, Y.; Haran, K. A High-Speed, High-Frequency, Air-Core PM Machine for Aircraft Application. In Proceedings of the 2016 IEEE Power and Energy Conference at Illinois (PECI), Urbana, IL, USA, 19–20 February 2016; pp. 1–4.
126. Yoon, A.; Xiao, J.; Lohan, D.; Arastu, F.; Haran, K. High-Frequency Electric Machines for Boundary Layer Ingestion Fan Propulsor. *IEEE Trans. Energy Convers.* **2019**, *34*, 2189–2197. [CrossRef]
127. Felder, J.L. NASA N3-X with Turboelectric Distributed Propulsion. 2014. Available online: https://ntrs.nasa.gov/api/citations/20150002081/downloads/20150002081.pdf (accessed on 28 July 2024).
128. Fard, M.T.; He, J.; Huang, H.; Cao, Y. Aircraft Distributed Electric Propulsion Technologies—A Review. *IEEE Trans. Transp. Electrif.* **2022**, *8*, 4067–4090. [CrossRef]
129. Gao, H.; Zhang, Z.; Liu, Y.; Huang, W.; Xue, H. Development and Analysis of Dual Three-Phase PMSM With Phase-Shifted Hybrid Winding for Aircraft Electric Propulsion Application. *IEEE Trans. Transp. Electrif.* **2024**, *10*, 6497–6508. [CrossRef]
130. Felder, J.; Kim, H.; Brown, G. Turboelectric Distributed Propulsion Engine Cycle Analysis for Hybrid-Wing-Body Aircraft. In Proceedings of the 47th AIAA Aerospace Sciences Meeting Including the New Horizons Forum and Aerospace Exposition, Orlando, FL, USA, 5–8 January 2009.
131. Felder, J.L.; Brown, G.V.; DaeKim, H.; Chu, J. Turboelectric Distributed Propulsion in a Hybrid Wing Body Aircraft. In Proceedings of the 20th International Society for Airbreathing Engines (ISABE 2011), Gothenburg, Sweden, 12–16 September 2011; Available online: https://ntrs.nasa.gov/citations/20120000856 (accessed on 28 July 2024).
132. Terao, Y.; Akasaka, K.; Ohsaki, H.; Okai, K.; Taguchi, H. Electromagnetic Analysis of Fully Superconducting Motors Employing Dilute Gas Rotor and Liquid Hydrogen Stator Cooling Structure. *J. Phys. Conf. Ser.* **2023**, *2545*, 012027. [CrossRef]
133. Thuries, E.; Pham, V.D.; Laumond, Y.; Verhaege, T.; Fevrier, A.; Collet, M.; Bekhaled, M. Towards the Superconducting Fault Current Limiter. *IEEE Trans. Power Deliv.* **1991**, *6*, 801–808. [CrossRef]
134. Masson, P.J.; Tixador, P.; Luongo, C.A. Safety Torque Generation in HTS Propulsion Motor for General Aviation Aircraft. *IEEE Trans. Appl. Supercond.* **2007**, *17*, 1619–1622. [CrossRef]
135. Constantinides, S.; Maybury, D.; Wyss, U.; Martinek, G. Extending the Limits of the Sm2Co17 System. Available online: https://www.magmatllc.com/PDF/Extending%20the%20limits%20of%20the%20Sm2Co17%20System%20-%20160629sc%20-%20Final%20edit.pdf (accessed on 1 October 2024).
136. Rom, C.L.; Smaha, R.W.; O'Donnell, S.; Dugu, S.; Bauers, S.R. Emerging Magnetic Materials for Electric Vehicle Drive Motors. *MRS Bull.* **2024**, *49*, 738–750. [CrossRef]
137. Cui, J.; Kramer, M.; Zhou, L.; Liu, F.; Gabay, A.; Hadjipanayis, G.; Balasubramanian, B.; Sellmyer, D. Current Progress and Future Challenges in Rare-Earth-Free Permanent Magnets. *Acta Mater.* **2018**, *158*, 118–137. [CrossRef]
138. Sugita, Y.; Mitsuoka, K.; Komuro, M.; Hoshiya, H.; Kozono, Y.; Hanazono, M. Giant Magnetic Moment and Other Magnetic Properties of Epitaxially Grown Fe16N2 Single-Crystal Films (Invited). *J. Appl. Phys.* **1991**, *70*, 5977–5982. [CrossRef]
139. Liu, J.; Guo, G.; Zhang, X.; Zhang, F.; Ma, B.; Wang, J.-P. Synthesis of A″-Fe16N2 Foils with an Ultralow Temperature Coefficient of Coercivity for Rare-Earth-Free Magnets. *Acta Mater.* **2020**, *184*, 143–150. [CrossRef]
140. Electrical Resistivity and Conductivity. Wikipedia 2024. Available online: https://en.wikipedia.org/wiki/Electrical_resistivity_and_conductivity (accessed on 28 July 2024).

141. Selema, A.; Ibrahim, M.N.; Sergeant, P. Electrical Machines Winding Technology: Latest Advancements for Transportation Electrification. *Machines* **2022**, *10*, 563. [CrossRef]
142. Manolopoulos, C.D.; Iacchetti, M.F.; Smith, A.C.; Miller, P.; Husband, M. Litz Wire Loss Performance and Optimization for Cryogenic Windings. *IET Electr. Power Appl.* **2023**, *17*, 487–498. [CrossRef]
143. Wei, B.Q.; Vajtai, R.; Ajayan, P.M. Reliability and Current Carrying Capacity of Carbon Nanotubes. *Appl. Phys. Lett.* **2001**, *79*, 1172–1174. [CrossRef]
144. Pyrhönen, J.; Montonen, J.; Lindh, P.; Vauterin, J.J.; Otto, M. Replacing Copper with New Carbon Nanomaterials in Electrical Machine Windings. *Int. Rev. Electr. Eng. IREE* **2015**, *10*, 12. [CrossRef]
145. Rallabandi, V.; Taran, N.; Ionel, D.M.; Eastham, J.F. On the Feasibility of Carbon Nanotube Windings for Electrical Machines—Case Study for a Coreless Axial Flux Motor. In Proceedings of the 2016 IEEE Energy Conversion Congress and Exposition (ECCE), Milwaukee, WI, USA, 18–22 September 2016; pp. 1–7.
146. Landi, B.; Cress, C.; Zeira, E.; Schauer, M.; Kukowski, T.; Leggiero, A.; McIntyre, D. *Nanometal-Interconnected Carbon Conductors (NICCS) for Advanced Electric Machines (RIT Final Technical Report)*; Rochester Inst. of Technology: Rochester, NY, USA, 2020.
147. Jiang, H.; Cooke, L.; Srivilliputhur, K.; McGuire, M.A.; Meyer, H.M.I.; Yoon, M.; Haynes, J.; Nawaz, K.; Lupini, A.R.; Li, K.; et al. Copper–Carbon Nanotube Composites Enabled by Brush Coating for Advanced Conductors. *ACS Appl. Nano Mater.* **2024**, *7*, 11176–11183. [CrossRef]
148. O'Donnell, D.; Bartos, S.; Tjong, J.; Kar, N.C. Utilization of Innovative Materials toward Permanent Magnet Synchronous E-Motors for Traction Application: A Review. In Proceedings of the 2020 2nd International Conference on Smart Power & Internet Energy Systems (SPIES), Bangkok, Thailand, 15–18 September 2020; pp. 380–385.
149. Boubaker, N.; Matt, D.; Enrici, P.; Nierlich, F.; Durand, G. Measurements of Iron Loss in PMSM Stator Cores Based on CoFe and SiFe Lamination Sheets and Stemmed From Different Manufacturing Processes. *IEEE Trans. Magn.* **2019**, *55*, 1–9. [CrossRef]
150. Cossale, M.; Krings, A.; Soulard, J.; Boglietti, A.; Cavagnino, A. Practical Investigations on Cobalt–Iron Laminations for Electrical Machines. *IEEE Trans. Ind. Appl.* **2015**, *51*, 2933–2939. [CrossRef]
151. Prabhu, M.A.; Loh, J.Y.; Joshi, S.C.; Viswanathan, V.; Ramakrishna, S.; Gajanayake, C.J.; Gupta, A.K. Magnetic Loading of Soft Magnetic Material Selection Implications for Embedded Machines in More Electric Engines. *IEEE Trans. Magn.* **2016**, *52*, 1–6. [CrossRef]
152. Krings, A.; Cossale, M.; Tenconi, A.; Soulard, J.; Cavagnino, A.; Boglietti, A. Characteristics Comparison and Selection Guide for Magnetic Materials Used in Electrical Machines. In Proceedings of the 2015 IEEE International Electric Machines & Drives Conference (IEMDC), Coeur d'Alene, ID, USA, 10–13 May 2015; pp. 1152–1157.
153. Stanley, J.K.; Yensen, T.D. Hiperco—A Magnetic Alloy. *Trans. Am. Inst. Electr. Eng.* **1947**, *66*, 714–718. [CrossRef]
154. Bozorth, R.M. *Ferromagnetism*; IEEE Press: Piscataway, NJ, USA, 1993; ISBN 978-0-7803-1032-2.
155. Mehedi, M.; Jiang, Y.; Suri, P.K.; Flannigan, D.J.; Wang, J.-P. Minnealloy: A New Magnetic Material with High Saturation Flux Density and Low Magnetic Anisotropy. *J. Phys. Appl. Phys.* **2017**, *50*, 37LT01. [CrossRef]
156. Sundar, R.S.; Deevi, S.C.; Reddy, B.V. High Strength FeCo–V Intermetallic Alloy: Electrical and Magnetic Properties. *J. Mater. Res.* **2005**, *20*, 1515–1522. [CrossRef]
157. Thao, N.G.M.; Fujisaki, K.; Mamiya, H.; Kuroda, S.; Yamabe-Mitarai, Y.; Motohashi, N. Magnetic Characterization of 4 μm-Thick Steel Made by Continuous Rolling Process for Power Electronic Applications in High Frequency. *IEEJ J. Ind. Appl.* **2021**, *10*, 731–739. [CrossRef]
158. Zhao, H.; Lin, N.; Zhang, J.; Wang, D.; Wang, Y.; Yu, X.; Chen, J. A Low-Loss High Saturation Fe-Co Alloy for High Power Density Aircraft Electric Motors. *IEEE Trans. Appl. Supercond.* **2024**, *34*, 1–6. [CrossRef]
159. Trnka, N.; Schleicher, A.; Lorenz, F.; Werner, R. Reduction of Eddy Current Losses in Stacked Laminations via Electrochemical Deburring. In Proceedings of the IKMT 2022; 13. GMM/ETG-Symposium, Linz, Austria, 14–15 September 2022; pp. 1–6.
160. El-Refaie, A. Role of Advanced Materials in Electrical Machines. *CES Trans. Electr. Mach. Syst.* **2019**, *3*, 124–132. [CrossRef]
161. Gloria, A.; Montanari, R.; Richetta, M.; Varone, A. Alloys for Aeronautic Applications: State of the Art and Perspectives. *Metals* **2019**, *9*, 662. [CrossRef]
162. D'Errico, F.; Tauber, M.; Just, M. Magnesium Alloys for Sustainable Weight-Saving Approach: A Brief Market Overview, New Trends, and Perspectives. In *Current Trends in Magnesium (Mg) Research*; IntechOpen: London, UK, 2022; ISBN 978-1-80355-481-5.
163. Kurzynowski, T.; Pawlak, A.; Smolina, I. The Potential of SLM Technology for Processing Magnesium Alloys in Aerospace Industry. *Arch. Civ. Mech. Eng.* **2020**, *20*, 23. [CrossRef]
164. Koch, S.-F.; Peter, M.; Fleischer, J. Lightweight Design and Manufacturing of Composites for High-Performance Electric Motors. *Procedia CIRP* **2017**, *66*, 283–288. [CrossRef]
165. Reuter, S.; Langheck, A.; Liebertseder, J.; Doppelbauer, M. Influence of Lightweight Plastic Stator Housing on the NVH Behavior of High-Performance Electric Machines. In Proceedings of the Electromechanical Drive Systems 2021, ETG Symposium, Online, 9–10 November 2021; pp. 1–7.
166. Oliver, J.A.; Guerrero, G.; Goldman, J. Ceramic Bearings for Electric Motors: Eliminating Damage with New Materials. *IEEE Ind. Appl. Mag.* **2017**, *23*, 14–20. [CrossRef]
167. Iosif, V.; Roger, D.; Takorabet, N.; Duchesne, S.; Meibody-Tabar, F. Technological Assessments for Designing Machines Able to Work at Very High Internal Temperatures (450–500 °C). In Proceedings of the 2016 XXII International Conference on Electrical Machines (ICEM), Lausanne, Switzerland, 4–7 September 2016; pp. 2682–2687.

168. Cozonac, D.; Babicz, S.; Ait-Amar-Djennad, S.; Velu, G.; Cavalini, A.; Wang, P. Study on Ceramic Insulation Wires for Motor Windings at High-Temperature. In Proceedings of the 2014 IEEE Conference on Electrical Insulation and Dielectric Phenomena (CEIDP), Des Moines, IA, USA, 19–22 October 2014; pp. 172–175.
169. Kadim, E.J.; Noorden, Z.A.; Adzis, Z.; Azis, N. Nanoparticles Application in High Voltage Insulation Systems. *IEEE Trans. Dielectr. Electr. Insul.* **2021**, *28*, 1380–1399. [CrossRef]
170. Shin, E.-S.E. Development of High Voltage Micro-Multilayer Multifunctional Electrical Insulation (MMEI) System. In Proceedings of the 2019 AIAA/IEEE Electric Aircraft Technologies Symposium (EATS), Indianapolis, IN, USA, 22–24 August 2019; pp. 1–14.
171. Pang, Y.; Hodgson, S.N. Nanocomposite Coatings for High Temperature Insulation of Electrical Wires. 2018. Available online: https://research.tees.ac.uk/files/8653886/AEM2018_abstract.pdf (accessed on 6 July 2024).
172. Miersch, S.; Schubert, R.; Schuhmann, T.; Schuffenhauer, U.; Buddenbohm, M.; Beyreuther, M.; Kuhn, J.; Lindner, M.; Cebulski, B.; Jung, J. Ceramic-like Composite Systems for Winding Insulation of Electrical Machines. In Proceedings of the 2020 International Conference on Electrical Machines (ICEM), Gothenburg, Sweden, 23–26 August 2020; Volume 1, pp. 1540–1546.
173. Yin, W.; Yakimov, A.; Comanzo, H.; Siclovan, O.; Smigelski, P.; Gao, J.; Bodla, K.; Duggal, A. Highly Thermally Conductive Insulation for High Power Density Electric Machines. In Proceedings of the 2019 AIAA/IEEE Electric Aircraft Technologies Symposium (EATS), Indianapolis, IN, USA, 22–24 August 2019; pp. 1–7.
174. Pan, X.-F.; Bao, Z.; Xu, W.; Gao, H.-L.; Wu, B.; Zhu, Y.; Yu, G.-H.; Chen, J.; Zhang, S.-C.; Li, L.; et al. Recyclable Nacre-Like Aramid-Mica Nanopapers with Enhanced Mechanical and Electrical Insulating Properties. *Adv. Funct. Mater.* **2023**, *33*, 2210901. [CrossRef]
175. Properties of Nomex® 410 | DuPont™ Nomex® Insulation | DuPont USA. Available online: https://www.dupontdenemours.be/fr/news/nomex-410.html (accessed on 3 October 2024).
176. Wrobel, R.; Hussein, A. Design Considerations of Heat Guides Fabricated Using Additive Manufacturing for Enhanced Heat Transfer in Electrical Machines. In Proceedings of the 2018 IEEE Energy Conversion Congress and Exposition (ECCE), Portland, OR, USA, 23–27 September 2018; pp. 6506–6513.
177. Wong, M.; Owen, I.; Sutcliffe, C.J.; Puri, A. Convective Heat Transfer and Pressure Losses across Novel Heat Sinks Fabricated by Selective Laser Melting. *Int. J. Heat Mass Transf.* **2009**, *52*, 281–288. [CrossRef]
178. Lammers, S.; Adam, G.; Schmid, H.J.; Mrozek, R.; Oberacker, R.; Hoffmann, M.J.; Quattrone, F.; Ponick, B. Additive Manufacturing of a Lightweight Rotor for a Permanent Magnet Synchronous Machine. In Proceedings of the 2016 6th International Electric Drives Production Conference (EDPC), Nuremberg, Germany, 30 November–1 December 2016; pp. 41–45.
179. Wrobel, R.; Mecrow, B. Additive Manufacturing in Construction of Electrical Machines—A Review. In Proceedings of the 2019 IEEE Workshop on Electrical Machines Design, Control and Diagnosis (WEMDCD), Athens, Greece, 22–23 April 2019; Volume 1, pp. 15–22.
180. Tomlin, M.; Meyer, J. Topology Optimization of an Additive Layer Manufactured (ALM) Aerospace Part. Available online: https://www.additivemanufacturing.media/cdn/cms/uploadedFiles/Topology-Optimization-of-an-Additive-Layer-Manufactured-Aerospace-Part.pdf (accessed on 5 October 2024).
181. Volegov, A.S.; Andreev, S.V.; Selezneva, N.V.; Ryzhikhin, I.A.; Kudrevatykh, N.V.; Mädler, L.; Okulov, I.V. Additive Manufacturing of Heavy Rare Earth Free High-Coercivity Permanent Magnets. *Acta Mater.* **2020**, *188*, 733–739. [CrossRef]
182. Gargalis, L.; Madonna, V.; Giangrande, P.; Rocca, R.; Hardy, M.; Ashcroft, I.; Galea, M.; Hague, R. Additive Manufacturing and Testing of a Soft Magnetic Rotor for a Switched Reluctance Motor. *IEEE Access* **2020**, *8*, 206982–206991. [CrossRef]
183. Wang, J.; Yuan, X.; Riipinen, T.; Pippuri-Mäkeläinen, J.; Metsä-Kortelainen, S.; Lindroos, T. Evaluation of 3D Printed Cobalt Iron Cores for Filter Inductors. *IEEE Trans. Magn.* **2020**, *56*, 1–5. [CrossRef]
184. Garibaldi, M.; Gerada, C.; Ashcroft, I.; Hague, R. Free-Form Design of Electrical Machine Rotor Cores for Production Using Additive Manufacturing. *J. Mech. Des.* **2019**, *141*, 071401. [CrossRef]
185. Wu, F.; EL-Refaie, A.M.; Al-Qarni, A. Minimization of Winding AC Losses Using Inhomogeneous Electrical Conductivity Enabled by Additive Manufacturing. *IEEE Trans. Ind. Appl.* **2022**, *58*, 3447–3458. [CrossRef]
186. Lorenz, F.; Rudolph, J.; Wemer, R. Design of 3D Printed High Performance Windings for Switched Reluctance Machines. In Proceedings of the 2018 XIII International Conference on Electrical Machines (ICEM), Alexandroupoli, Greece, 3–6 September 2018; pp. 2451–2457.
187. Kapuściński, J.; Domański, R. Method for Efficient Feasibility Study of Air Cooling Systems for Modern PMSM Electric Motors in All-Electric Aviation. *J. Mech. Energy Eng.* **2020**, *4*, 89–96. [CrossRef]
188. Madonna, V.; Walker, A.; Giangrande, P.; Serra, G.; Gerada, C.; Galea, M. Improved Thermal Management and Analysis for Stator End-Windings of Electrical Machines. *IEEE Trans. Ind. Electron.* **2019**, *66*, 5057–5069. [CrossRef]
189. Wrobel, R.; Mecrow, B.; Benarous, M. Thermal Evaluation of a Short-Operating-Duty Dual-Lane Fault-Tolerant Actuator for Aerospace Applications. *IEEE Trans. Ind. Appl.* **2023**, *59*, 4083–4094. [CrossRef]
190. Liao, C.; Zhang, Z.; Han, J.; Zhang, J.; Wang, C.; Wang, P. Analysis and Efficient Calculation of the Magnet Eddy Current Loss of PMSM. *IEEE Trans. Ind. Appl.* **2024**, *60*, 8797–8806. [CrossRef]
191. Wang, H.; Liu, X.; Kang, M.; Guo, L.; Li, X. Oil Injection Cooling Design for the IPMSM Applied in Electric Vehicles. *IEEE Trans. Transp. Electrif.* **2022**, *8*, 3427–3440. [CrossRef]
192. Jones, E.G.; Balster, W.J.; Balster, L.M. Aviation Fuel Recirculation and Surface Fouling. *Energy Fuels* **1997**, *11*, 1303–1308. [CrossRef]

193. Ferreira, C.A.; Richter, E. *Detailed Design of a 250-kW Switched Reluctance Starter/Generator for an Aircraft Engine*; SAE International: Warrendale, PA, USA, 1993.
194. Wrobel, R.; MGlen, R.J. Heat Pipes in Thermal Management of Electrical Machines—A Review. *Therm. Sci. Eng. Prog.* **2021**, *26*, 101053. [CrossRef]
195. Wan, Z.; Sun, B.; Wang, X.; Wen, W.; Tang, Y. Improvement on the Heat Dissipation of Permanent Magnet Synchronous Motor Using Heat Pipe. *Proc. Inst. Mech. Eng. Part J. Automob. Eng.* **2020**, *234*, 1249–1259. [CrossRef]
196. Putra, N.; Ariantara, B. Electric Motor Thermal Management System Using L-Shaped Flat Heat Pipes. *Appl. Therm. Eng.* **2017**, *126*, 1156–1163. [CrossRef]
197. Wrobel, R. A Technology Overview of Thermal Management of Integrated Motor Drives—Electrical Machines. *Therm. Sci. Eng. Prog.* **2022**, *29*, 101222. [CrossRef]